إقرار

أنا الموقع أدناه مقدم الرسالة التي تحمل العنوان:

الخلايا الشمسية الصبغية المعتمدة على الصبغات المستخلصة من جذور النباتات

Dye sensitized solar cells based on natural dyes extracted from plant roots

أقر بأن ما اشتملت عليه هذه الرسالة إنما هي نتاج جهدي الخاص، باستثناء ما تمت الإشارة إليه حيثما ورد، وإن هذه الرسالة ككل، أو أي جزء منها لم يقدم من قبل لنيل درجة أو لقب علمي أو بحثي لدى أية مؤسسة تعليمية أو بحثية أخرى.

DECLARATION

The work provided in this thesis, unless otherwise referenced, is the researcher's own work, and has not been submitted elsewhere for any other degree or qualification

اسم الطالب: إسلام محمود حسانين رضوان Student's name:

التوقيع: Signature

التاريخ: ٢٦/٤/٢٠١٥م Date:

Islamic University of Gaza
Deanery of Higher Studies
Faculty of Science
Department of Physics

Dye Sensitized Solar Cells Based on Natural Dyes Extracted from Plant Roots

الخلايا الشمسية الصبغية المعتمدة على الصبغات المستخلصة من جذور النباتات

By

Islam Mahmoud Radwan

B.Sc. in Physics, Islamic University of Gaza

Supervisors

Dr. Taher M. El-Agez
Associate Professor of Physics

Dr. Sofyan A. Taya
Associate Professor of Physics

Submitted to the Faculty of Science as a Partial Fulfillment of the Master Degree of Science (M. Sc.) in Physics

1436 – 2015

بسم الله الرحمن الرحيم

الجامعة الإسلامية – غزة
The Islamic University - Gaza

مكتب نائب الرئيس للبحث العلمي والدراسات العليا هاتف داخلي: 1150

الرقم Ref ج س غ/35/.....

التاريخ Date 2015/04/04.....

نتيجة الحكم على أطروحة ماجستير

بناءً على موافقة شئون البحث العلمي والدراسات العليا بالجامعة الإسلامية بغزة على تشكيل لجنة الحكم على أطروحة الباحث/ **اسلام محمود حسان رضوان** لنيل درجة الماجستير في **كلية العلوم قسم الفيزياء** وموضوعها:

الخلايا الشمسية الصبغية المعتمدة على الصبغات المستخلصة من جذور النباتات

Dye sensitized solar cells based on natural dyes extracted from plant roots

وبعد المناقشة العلنية التي تمت اليوم السبت 15 جمادى الآخر 1436هـ، الموافق 2015/04/04 الساعة الثانية عشرة ظهراً بمبنى القدس، اجتمعت لجنة الحكم على الأطروحة والمكونة من:

د. طاهر محمد العاجز	مشرفًا ورئيساً	.....
د. سفيان عبد الرحمن تايه	مشـــــرفاً	.....
أ.د. ناصر إسماعيل فرحات	مناقشًا داخلياً	.....
د. أمل محمود الكحلوت	مناقشًا خارجياً	.....

وبعد المداولة أوصت اللجنة بمنح الباحث درجة الماجستير في **كلية العلوم/ قسم الفيزياء.**

واللجنة إذ تمنحه هذه الدرجة فإنها توصيه بتقوى الله ولزوم طاعته وأن يسخر علمه في خدمة دينه ووطنه.

والله ولي التوفيق،،،

مساعد نائب الرئيس للبحث العلمي والدراسات العليا

أ.د. فؤاد علي العاجز

P.O. Box 108, Rimal, Gaza, Palestine fax: +970 (8) 286 0800 فاكس Tel: +970 (8) 286 0700 ص.ب. 108 الرمال، غزة، فلسطين هاتف
public@iugaza.edu.ps www.iugaza.edu.ps

Dedication

I dedicate my thesis to:

The sake of Allah, my greatest Creator,

My beloved messenger, Mohammed (Peace be upon him),

My beautiful homeland, Palestine,

Our martyrs and prisoners who sacrificed their lives for the sake of Palestine,

The Islamic University of Gaza (IUG),

My loving parents who kept supporting me throughout the process,

My dearest wife and son who stood by me in my difficult time,

My dear brothers and sisters,

My friends who encouraged and supported me.

Islam M. Radwan

Acknowledgment

In the Name of Allah, the Most Merciful, the Most compassionate, I must acknowledge my thanks to the greatest Allah, for His bless and guidance. I owe my university, IUG, the success of my work.

I am very grateful to all people who never hesitated to give me a hand to complete my research, particularly Dr. Sofyan Taya and Dr. Taher El-Agez.

I would like to thank the staff members in Physics department at IUG for their continued support. I would like to express my special thanks to my dear friends who helped me pursue my thesis.

Abstract

The objectives of this thesis are to prepare dye sensitized solar cells (DSSCs) using titanium dioxide (TiO_2) as a semiconducting layer based on six natural dyes extracted from plant roots which are purple carrot, carrot, beet, curcuma, kale and radish as sensitizers. Among the previous dyes, purple carrot showed the best efficiency.

The performance of DSSCs sensitized by purple carrot is improved through: adjustment of the solution extraction temperature, studying the effect of pH on the extract solution, and finally the influence of pre and post-treatments of the fluorinated tin oxide (FTO) glass substrate and the TiO_2 film using hydrochloric (HCl), phosphoric (H_3PO_4), and nitric (HNO_3) acids.

The results showed that an extracting temperature of 50°C could be used as an optimal value. The treatment of the dye solutions with acetic acid resulted in better performance in comparison with the hydrochloric acid treatment. The pre-treatment of the FTO with H_3PO_4 and the post-treatment of TiO_2 with HNO_3 resulted in improved efficiencies of 130% and 250% respectively for the DSSCs sensitized by purple carrot.

Abstract in Arabic

إن أهداف هذا البحث تتمثل في تحضير خلايا شمسية صبغية باستخدام ثاني أكسيد التيتانيوم كطبقة شبه موصلة معتمدة على 6 صبغات طبيعية مستخلصة من جذور النباتات وهي الجزر الأرجواني، البنجر، الكركم، الجزر، اللفت، والفجل. من بين هذه الجذور أظهر الجزر الأرجواني أعلى كفاءة.

ولقد تم تحسين أداء الخلايا الشمسية الصبغية المستخلصة من صبغة الجزر الأرجواني من خلال: ضبط درجة حرارة استخلاص الصبغة، ودراسة تأثير تغيير درجة الحموضة للمحلول المستخلص، وأخيرا دراسة المعالجة لسطح FTO وطبقة شبه الموصل TiO_2 باستخدام أحماض الهيدروكلوريك (HCl)، الفوسفوريك (H_3PO_4)، والنيتريك (HNO_3).

وتظهر النتائج أن درجة الحرارة 50س يمكن استعمالها كقيمة مثلى لاستخلاص الصبغة. وجدير بالذكر أنه تم الوصول لأداء أفضل بمعالجة محلول الصبغة باستخدام حمض الأستيك (الخليك) مقارنة بحمض الهيدروكلوريك. من الواضح أن الخلايا الشمسية الصبغية المستخلصة من صبغة الجزر الأرجواني أظهرت كفاءة بنسبة 130% نتيجة المعالجة لسطح الزجاج باستخدام حمض الفوسفوريك. في حين أن المعالجة لطبقة شبه الموصل TiO_2 باستخدام حمض النيتريك أظهر زيادة كفاءة الخلية بنسبة 250 %.

CONTENTS

List of Figures

List of Tables

List of Abbreviations

A	Absorbance
AC	Alternative Current
a.u.	Arbitrary units
a-Si	Amorphous silicon
ACN	Acetonitrile
AM 1.5 G	Air mass 1.5 global spectrum
CB	Conduction band
Cd-Te	Cadmium Telluride
CE	Counter electrode
CIGS	Copper-Indium-Gallium-Diselenide
CIS	Copper-Indium-Selenide
CPE	Constant phase element
R_{CT}	Charge transfer resistance
CPV	Concentrating photovoltaic
c-Si	Crystalline silicon
DC	Direct current
DSSC	Dye sensitized solar cell
E_g	Energy bandgap
EIS	Electrochemical impedance spectroscopy
EPFL	Ecole Polytechnique Federale de Lausanne
EQE	External quantum efficiency
e^-	Electron

eV	Electron volt
f	Frequency
FF	Fill factor
FRA	Frequency response analyzer
FTO	Fluorine-doped tin oxide
h	Hour
H_3PO_4	Phosphoric acid
HCl	Hydrochloric acid
HNO_3	Nitric acid
HOMO	Highest occupied molecular orbital
I	Light intensity
I^-	Iodide
I_3^-	Tri-iodide
I_m	Current at the maximum power point
I_o	The intensity of the reference beam
IPCE	Incident photon to current conversion efficiency
ITO	Indium-doped tin oxide
IUG	Islamic university of Gaza
I-V	Current – Voltage
J_{sc}	Short circuit current density
J-V	Current density – Voltage
LUMO	Lowest unoccupied molecular orbital
mc-Si	Multi-crystalline Silicon

N719	Bis(tetrabutylammonium)cis-di(thiocyanato)bis(2,2′-bipyridine -4-COOH,4′-COO–)ruthenium(II)
ND.	Natural dye
OPV	Organic photovoltaic
^{o}C	Celsius degree
^{o}K	Kelvin degree
PEDOT	Poly (3,4-ethylenedioxythiophene)
PE	Photoelectrode
P_{in}	Power of incident light
P_{m}	Maximum power
P_{out}	Output power
Pt	Platinum
PV	Photovoltaic
R	Resistance
R_{S}	Series resistance
R_{shunt}	Shunt resistance
Ru	Ruthenium
S*	Excited energy state of the sensitizer
S^{+}	Oxidized state of the sensitizer
S_{0}	Ground energy state of the sensitizer
sc-Si	Single crystalline silicon
T	Temperature
T	Transmittance

TCO	Transparent conducting oxide
TiO_2	Titanium dioxide
US	United States of America
UV	Ultraviolet
UV-Vis	Ultraviolet-Visible
VB	Valence band
V_m	Maximum voltage
V_{oc}	Open circuit voltage
Z'	Real impedance
Z''	Imaginary impedance
Z_C	Capacitance impedance
Z_{im}	Imaginary impedance
ZnO	Zinc oxide
Z_R	Resistance impedance
Z_{re}	Real impedance
α	Absorption coefficient
η	Solar energy to electric power conversion efficiency
λ	Wavelength of the light
λ_{max}	Maximum wavelength
ε	Extinction coefficient
τ	Electron lifetime
ω	Angular frequency

CHAPTER ONE
1. INTRODUCTION

1.1. Global Energy Demand

The impressive increase in energy consumption is one of the most critical and greatest challenges we face today. With a constantly growing human population and improved living standards, more energy will be needed. Currently, the energy consumption estimate for seven billion people worldwide is about 14 terawatts (TW) and this is expected to go up by another 10 TW within the next 40 years [1]. For many years, the depletion of fossil fuel resources associated with the continually increasing demand is problematic. Mainly, energy from fossil fuels faces two major problems, the first is the limited resources and the second is their environmental impact. For these two reasons, there is increased global awareness concerning the urgent need to find alternative energy resources to meet our requirements. The supply of clean sustainable energy is considered as one of the most important scientific and technical challenges facing humanity in the 21st century [2].

1.2. Harvesting the Sun's Energy

"More energy from sunlight strikes Earth in 1 hour than all of the energy consumed by humans in an entire year" [3]. Sun has always been the most powerful energy source on earth since it satisfies all requirements of the energy source. It is clean, environmentally friendly and freely available. Sunlight can be transformed into electricity using solar cells. Solar cells have found applications in many different fields such as in calculators, solar lamps and even on spacecraft and satellites. The solar cell that currently has the largest share in the market is

based on crystalline silicon and was first reported by Chapin in 1954 [4]. Even if the efficiency since then has increased and the production cost decreased, it is still too expensive to be able to compete with the conventional energy sources. This has led to a great research interest in finding new ways of utilizing the solar energy with cheaper and more efficient methods.

1.3. Solar Radiation and Air Mass

The Sun can be considered as a black-body (an ideal diffuse emitter), emitting at 5500^{o}K. Its spectrum is very broad, stretching out from the X-rays up to the radio waves with the peak at 525 nm (2.36 eV). The atmosphere, protects the Earth surface from the excessive high energy radiation and affects the shape of the solar spectrum as shown in Fig. 1.1.

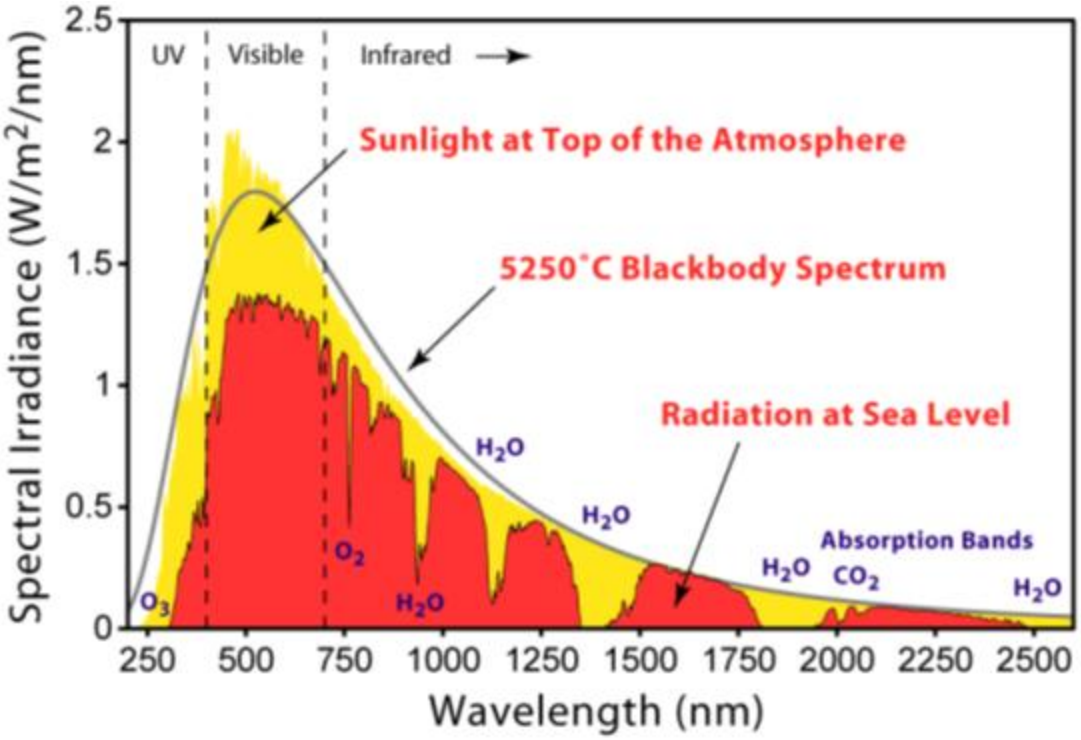

Fig. 1.1 A comparison of a black-body radiation at 5250°C (solid line) with the solar irradiance spectrum at the top of the Earth's atmosphere and after passing through the atmosphere [5].

The attenuation of the spectrum depends on the path length (atmosphere thickness). The coefficient that defines this direct optical path length is called air mass, AM which given by equation 1.1.

$$AM = \frac{1}{l_0} \approx \frac{1}{\cos z} \tag{1.1}$$

where l_0 is path length normal to the earth's surface at sea level and z is the zenith angle. The spectrum outside the atmosphere, is referred to as "AM0", meaning "zero atmospheres". And "AM1" is referred to the sun shining directly overhead at the sea level (z = 0°, the thickness of one atmosphere). Another very useful value is the "AM1.5", which corresponds to the zenith angle of 48.2°. Most of the human habitats are situated at the latitudes where the sun irradiation angle is close to that value (summer-winter variation, cloudy-sunny day variation), and in this way "AM1.5" represents the overall yearly average solar irradiation. Therefore, it is an important indicator for photovoltaic measurements, where the sun simulators ought to resemble the solar spectrum as close as possible to the reality. The specific value of 1.5 has been selected in the 1970s for standardization purposes, based on an analysis of solar irradiance data in the conterminous United States [6].

1.4. Generations of Photovoltaic Solar Cells

The photovoltaic (PV) effect was observed by Becquerel in 1839, who reported a current flow between two silver electrodes in an electrolyte media upon light exposure [7]. Photovoltaic comes from the words *photo* meaning light and *volt*, a measurement of electricity. Based on the nature of the material, maximum conversion efficiency obtainable, and the associated cost of photovoltaic power, Martin Green has grouped various

photovoltaic solar cells in three major categories.

1.4.1. First Generation of Photovoltaics (1970s)

Photovoltaic cells made from crystalline silicon (c-Si) were the first to find an important application in supplying satellites with energy. The choice of silicon was originally by its general use in the semiconductor industry. Silicon remains an attractive material, since it is one of the most abundant elements on earth (20% of the earth's crust), mainly in the form of sand (SiO_2). It is a semiconductor material suitable for PV applications, with energy band gap of 1.1 eV.

Crystalline silicon cells are classified into two main types depending on how the Si wafers are made.

1. Monocrystalline (Mono c-Si) sometimes also called single crystalline (sc-Si)
2. Polycrystalline (Poly c-Si), sometimes referred to as multi-crystalline (mc-Si)

Almost 90% of the World's photovoltaics today are based on some variation of silicon. Monocrystalline solar panels have the highest efficiency rates since they are made out of the highest-grade silicon. The efficiency rates of monocrystalline solar panels are typically 20-25%. Whereas the efficiency of polycrystalline-based solar panels is typically 13-16% [8]. Because of lower silicon purity, polycrystalline solar panels are not quite as efficient as monocrystalline solar panels.

These high efficiency technologies, however, generally incur higher production costs compared to standard silicon cells due to high labor costs for the material processing and the significant energy input required, cost per watt is also the highest.

1.4.2. Second Generation of Photovoltaics (1980s)

Conventional crystalline silicon technologies require a lot of effort, and numerous complex processing steps. Second generation technology aims to use layers of semiconductor materials only a few micrometers thick deposited on low-cost substrates such as glass, flexible plastic, or stainless steel whilst maintaining the efficiencies of the first generation of PV. As a consequence, they require less semiconductor material to manufacture in order to absorb the same amount of sunlight. In addition, thin films can be packaged into flexible and lightweight structures. The three primary types of thin-film solar cells that have been commercially developed are:

1. Amorphous silicon (a-Si)
2. Cadmium Telluride (Cd-Te)
3. Copper-Indium-Selenide (CIS) and Copper-Indium-Gallium-Diselenide (CIGS)

Depending on the technology, thin-film module prototypes have reached efficiencies between 7–15% [9].

Almost all of today's thin-film technology is based on amorphous silicon in which there is very little order to the arrangement of atoms. CdTe thin-film PV solar cells have lower production costs and higher cell efficiencies (15.8%) than amorphous silicon thin-film technologies [10]. This combination makes CdTe thin-films the most economical thin-film technology currently available. The compound CdTe has different qualities than the two elements, cadmium and tellurium, taken separately. Toxicity studies show that CdTe is less toxic than elemental cadmium. CIS and CIGS PV cells offer the highest efficiencies of all thin-film PV technologies. Current module efficiencies are in the range of 7% to 16%, but efficiencies of up to 20.3% have been achieved in the laboratory, close to that of c-Si cells

[11]. The race is now to increase the efficiency of commercial modules.

1.4.3. Third Generation of Photovoltaics (1990s)

In the last years, new concepts of solar cells were considered. These technologies mainly include concentrating photovoltaic technology, dye-sensitized solar cells (DSSCs), organic solar cells, and novel and emerging solar cell concepts, all of which are now known as third generation photovoltaics since they are designed to combine the advantages of both the first and second generation devices. Because of the low cost materials and easy fabrication, these technologies are expected to take a significant share in the fast growing photovoltaic areas.

1.4.3.1 Concentrating Photovoltaic Technology

The idea of a concentrating photovoltaic technology (CPV) is to use optical devices, such as lenses, mirrors, or other reflecting surfaces to concentrate direct sun light onto very small, highly efficient multi-junction solar cells. To be effective, the lenses need to be permanently oriented towards the sun, using solar trackers. Since CPV modules rely on direct sunlight, they need to be used in regions with clear skies and high direct solar irradiation like deserts to maximize the performance. Commercial CPV modules with silicon-based cells offer efficiency in the range of 20% to 25%. CPV based on multi-junction solar cells using III-V semiconductors have achieved laboratory efficiency of more than 40% [12].

1.4.3.2 Dye Sensitized Solar Cells (DSSC)

The spectral response of stable wide bandgap semiconductors like TiO_2 can be extended to visible light by sensitization with a dye. In this case free charge carriers are not generated by

bandgap excitation of the semiconductor, but by electron or hole injection from the excited dye. The great advantage of this new type of solar cell is its ease of fabrication from cheap materials and the consequently low price. The efficiency increase in the solid state version of DSSCs from about 5% to over 15 % have been reported within two years of time scale [13]. The main reason why efficiencies of DSSC are low is because there are very few dyes that can absorb a broad spectral range. Thousands of organic dyes have been studied and tested in order to design, synthesize and assemble nanostructured materials that will allow higher power conversion efficiencies for DSSCs.

1.4.3.3 Organic Solar Cells

Organic solar cells are composed of organic or polymer materials. They are inexpensive, but not very efficient. Organic PV module efficiencies are in the range 4% to 5% for commercial systems and 6% to 8% in the laboratory [14]. In addition to the low efficiency, a major challenge for organic solar cells is their instability over time. Organic cells can be applied to plastic sheets in a manner similar to the printing and coating industries, meaning that organic solar cells are lightweight and flexible, making them ideal for mobile applications and for fitting to a variety of surfaces. This makes them particularly useful for portable applications, a first target market for this technology. These properties will make organic PV modules attractive for building-integrated applications as it will expand the range of shapes and forms where PV systems can be applied. Another advantage is that the technology uses abundant, non-toxic materials and is based on a very scalable production process with high productivity.

1.4.3.4 Novel and Emerging Solar Cell Concepts

In addition to the third-generation technologies mentioned above, there are a number of novel solar cell technologies under development that use quantum dots/wires, quantum wells, or super lattice technologies. These technologies could achieve very high efficiencies by overcoming the thermodynamic limitations of conventional crystalline cells. However, these high efficiency approaches are in the fundamental materials research phase.

1.5 Photovoltaic Processes in a Solar Cell

The understanding of photovoltaic process requires an understanding of the primary mechanisms of charge carrier generation and mobility in these materials. In a bulk crystalline semiconductors, the highest occupied and lowest unoccupied molecular orbitals (HOMO and LUMO) of constituent atoms or molecules converge into valence and conduction bands. For intrinsic semiconductors the Fermi energy level lies in the middle of the bandgap. It is possible to dope a semiconductor in order to increase the concentration of one of the free carrier types. The semiconductor is then referred to as extrinsic. Depending on whether the doping atoms are (donor) or (acceptor), the extrinsic semiconductor is n-type or p-type. The Fermi level lies in the upper half of the forbidden gap which is close to the conduction band for an n- type semiconductor and in the lower half for a p-type semiconductor which close to the valence band. In a sandwich structure composed of an n-doped and p-doped semiconductors, charge separation occurs due to bending of the bands in the vicinity of the interface [15] as shown in Fig. 1.2.

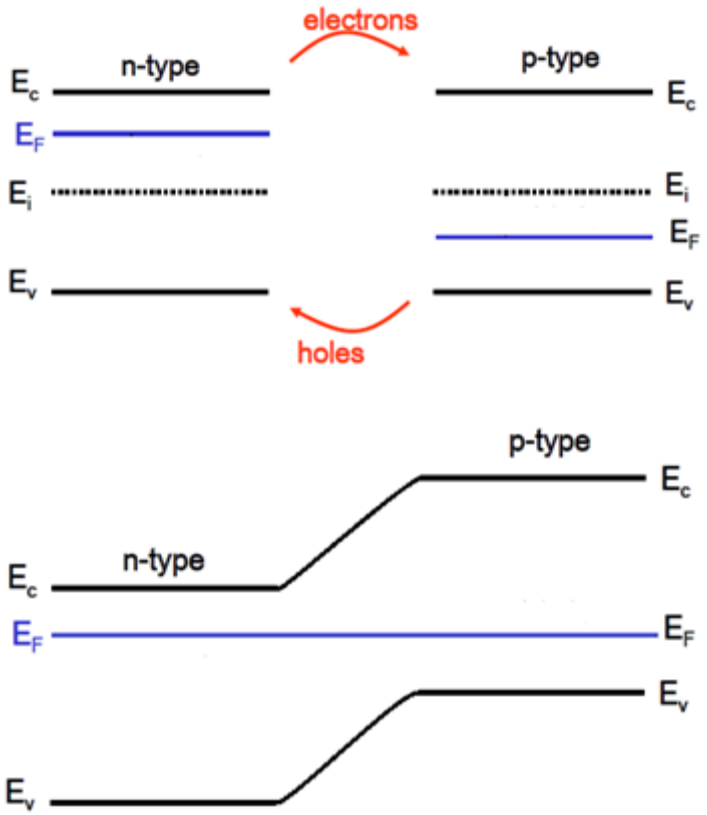

Fig. 1.2 Band Picture of n-type and p-type semiconductors with the indication of the Fermi level (E_f) before (upper scheme) and after joining (lower scheme) resulting in a p-n junction.

Optical excitation of the semiconductor with light of energy higher than the bandgap of the semiconductor leads to free charge carriers generation, electrons (e^-) and holes (h^+), and the single Fermi level splits into two quasi-Fermi levels in the n-type or p-type region respectively. These quasi-Fermi levels are now split; the higher the light intensity the more they split. Close to the electrode both quasi-Fermi levels collapse toward the majority quasi-Fermi levels, where they are connected. This shift of the Fermi levels in the electrodes represents the open circuit voltage, which can be approximated by the shift of the minority quasi-Fermi levels as shown in Fig. 1.3. Such separation of the charge carriers permits selective collection at the collector electrodes and a net conversion of sunlight to electric power [16].

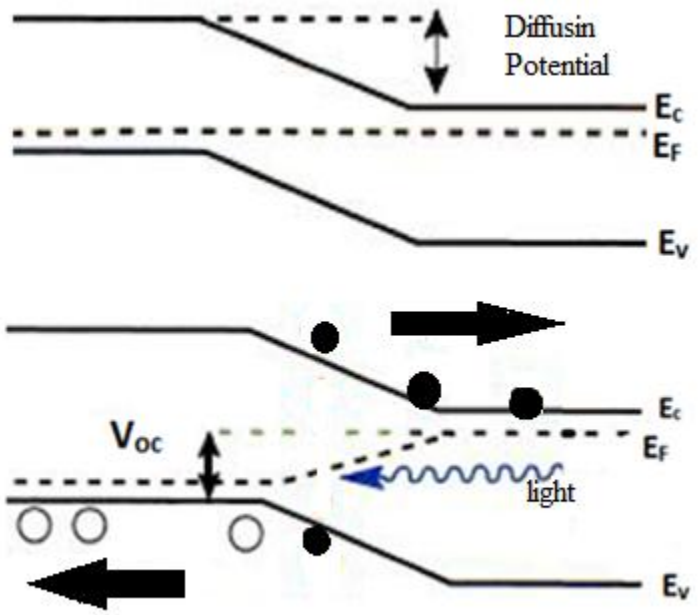

Fig. 1.3 The creation of the uniform Fermi level throughout the material results in the generation of the built-in potential (upper scheme) and the creation of electron-hole pairs when illuminated with light (lower scheme).

1.6 State of the Art

The concept of dye sensitization of wide bandgap semiconductors started in the late 1960s by the work of Gerischer [17] and Tsubomura [18] together with their co-workers where they used ZnO as the semiconductor and different dyes such as rose bengal as photosensitizer. As part of his PhD thesis work, Spitler later studied the excited state and charge injection of rose bengal onto a single crystal TiO_2 electrode [19]; However, the efficiencies remained low for many years. The breakthrough in the field came when Michael Gratzel and Brian O'Regan presented their results in 1991 with an impressive overall efficiency higher than 7%, using a ruthenium based sensitizer and a porous TiO_2 layer as the semiconductor material [20].

In 1997, Nerine J. Cherepy et al. reported that a photoelectrochemical cell utilizing flavonoid anthocyanin dyes extracted from blackberries was shown to convert sunlight to electrical power at an efficiency of 0.56% under full sun [21].

Other natural dyes reached up to 1.7% efficiency sensitizing TiO_2 as a monolayer, which was stated to be among the highest efficiencies achieved with raw natural dyes [22].

In 2012, DSSCs were assembled by using natural dyes extracted from alkanet root where alkannin is the coloring pigment in alkanet root.

In 2013, Ecole Polytechnique Federale de Lausanne (EPFL), a Switzerland-based university, announced that a research team led by Michael Gratzel, developed a solid-state dye-sensitized solar cell (DSSC) with a conversion efficiency of 15% [23].

In 2013, the performances of natural dye-sensitized solar cells assembled using natural dyes, anthocyanin, extracted from the flowers of Rhododendron species with three different colors, pink, red and violet were investigated. The dyes were treated with nitric and acetic acids to examine their effects on the power conversion efficiency [24].

Dye-sensitized solar cells research in the Islamic University of Gaza began in 2010 by the search team of the energy unit at the university, headed by Taher El Agez.

1.7 Gaza and Electricity Crisis

Gaza Strip has been suffering from a chronic crisis in the supply of electricity. This crisis is associated with political and economic conditions. The demand for electricity supply of Gaza Strip is estimated in the range between 350 and 450 MW depending on the season which is expected to rise up in case of lifting the (Israeli) siege. There are three primary sources which provide Gaza with electricity. First, 120 MW of the electrical supply to Gaza Strip is provided by the (Israeli) electricity company via ten electric lines. Second, the power station in Gaza and its maximum production capacity is 140 MW though its actual average of production is only 80 MW due to its dependency on the amount of fuel available

for the production of electricity. Third, the Egyptian electricity grid that supplies Gaza with around 27 MW through two main electric lines.

This means that only 230 MW of the electricity quantity available from the three sources. Accordingly, this shows a large deficit up to more than 150MW, representing 30 % of the total needs of electricity, which is largely influenced by the change in the supply and demand causing a power failure.

Since Gaza strip primarily depends on (Israel) for the import of electricity and fossil fuel, both acquired at high prices not justified by the economic distress conditions imposed locally. Energy and other resources have become means in achieving political aims. As a result, Gaza has been deprived of fossil fuel and electricity supply for several months. The majority of Gaza households have power cuts of at least eight hours per day. Some have no electricity for long as 12 hours a day.

The geographical location of Gaza Strip makes it a relatively sun-rich region with an annual solar irradiance of about 2000 kWh/m^2 [25]. This implies that the utilization of solar energy would be feasible and efficient enough for domestic, commercial, public and industrial applications. With the high electric power shortages at Gaza Strip, it seems that solar energy systems are attractive means to power some applications in various areas in Gaza Strip. Turning to exploiting of solar energy as main or even as standby sources of power will help ease the pressure on the distribution grid and will make more power available to the utility grid to supply more customers.

1.8 Research Aims

The aims of this thesis were to use natural dyes extracted from plant roots as sensitizers for

DSSCs, and to determine the best dye among several dyes have been tested. Also to optimize the extracting temperature of the purple carrot extracts, and to study the effects of the pH of the extract solution, pre-treatment of FTO glass substrate using different acids and finally post-treatment of TiO_2 on DSSCs performance.

1.9 Thesis Layout

The thesis is divided into five chapters. The first one gives an introduction to the thesis by describing the background and the general overview of the current photovoltaic technologies and briefly mention the state of the art concepts and the purpose of the study as well as the outline of the thesis. Chapter 2 explains the dye-sensitized solar cell beginning with the components of a DSSC then a short description of the operating principle of the cell and the parameters related to the DSSC. Finally, theoretical background of electrochemical impedance spectroscopy is introduced. Experimental techniques and DSSC preparation are presented in chapter 3. Chapter 4 introduces the experimental work for each study of the thesis. The experimental results are presented and discussed in chapter 4. Chapter 5 presents general conclusions, which is the summary of all previous chapters.

CHAPTER TWO

2. DYE SENSITIZED SOLAR CELLS

In the first part of this chapter, dye sensitized solar cells (DSSCs) and their components are presented. A DSSC is a successful combination of few materials, designed on a molecular level (dye), nanoscale (TiO_2 film) and in a macroscopic view (electrolyte). The second part of this chapter deals with the operation principle of DSSC and enlist the processes that happen during the cell's operation and highlights all the steps from the photon absorption to current extraction.

2.1 Introduction

A DSSC belongs to the third generation photovoltaic cells. It uses molecules to absorb photons and separates the two functions of light harvesting and charge transport. As one of the most important advantages of this type of solar cells is their suitability for many of the materials, and the possibility of production under mild conditions, making it significantly less expensive than the earlier cell design.

2.2 The Architecture of a DSSC

The DSSCs are made in a sandwich configuration of two pieces of conducting glass. The schematic representation of a DSSC is presented in the Fig. 2.1.

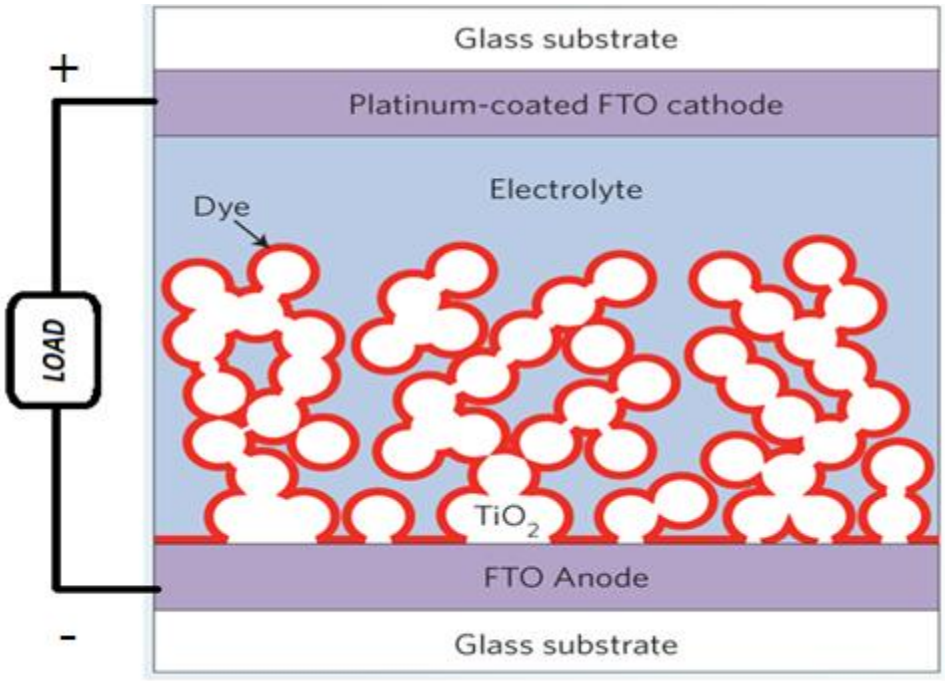

Fig. 2.1 A schematic representation of a dye-sensitized solar cell (DSSC).

2.3 Key Components of a Dye Sensitized Solar Cell

The main components of the cell are: a wide band gap semiconductor to which the dye is adsorbed and deposited on a transparent electrode (photoanode), electrolyte with a redox mediator and a counter-electrode.

2.3.1 Substrates

As mentioned earlier, the sandwich structure of the DSSC includes two transparent conducting glass substrates. Furthermore, in the case of front side illumination, the glass substrate acts also as a window for the incident light and should therefore be highly transparent in the visible-IR region. Blocking of UV light may be desired to prevent photodecomposition of the dye due to bandgap excitation of the semiconductor. The

substrate of the electrode serves as a collector for the current and therefore has to be well transparent conductor. On the other hand, the backside illumination through the counter electrode should has a reflecting photoelectrode (PE) substrate to enhance light absorption by reflecting back the transmitted light into the dye. The substrate is also the mechanical support for the very thin semiconductor coating, which should strongly adhere to it. Another requirement for the substrates is a low sheet resistance which should be temperature independent to the high temperatures (450-500^{o}C) used for the sintering process of the TiO_2 layer. Typical sheet resistance of the transparent conducting oxide (TCO) used is 5-15Ω/□ [9]. Both, indium-doped tin oxide (In:SnO_2, ITO) and fluorine doped tin oxide (F:SnO_2, FTO) have been used in DSSCs, however, due to poor thermal stability of the ITO layers, FTO glass is the preferred conducting substrate for the application in DSSCs.

2.3.2 TiO_2 Semiconductor as the Photoelectrode

A semiconductor is a material in which low concentrations of charge carriers can be produced either by thermal or photo-excitation, or by chemical doping. Intrinsic semiconductors are characterized by a fully occupied valence band and an empty conduction band. Intrinsic absorption of photons, whose energy is larger than the bandgap, produces electron-hole pairs. The DSSC revolution started actually from the application of the mesoporous TiO_2 layer consisting of 20 nm sized nanoparticles [20]. Some metal oxides such as TiO_2, SnO_2 or ZnO with energy band gap larger than 3 eV which called wide bandgap semiconductors and due to that they do not absorb visible light have been examined as potential electron acceptors for DSSCs. DSSC has a low efficiency of less than 1% until Gratzel employs porous TiO_2 as the anode material. Titania (TiO_2), a n-type semiconductor with a wide bandgap has been

well known and widely used in the photoanode of DSSCs. It offers some unique properties making it the preferred semiconductor for DSSCs. Its conduction band edge lies slightly below the excited state energy level of many dyes, which is one of the conditions for efficient electron injection. In 1985, Desilvestro showed that if TiO_2 is used in a nanoparticle form, the power conversion efficiency of DSSC can be drastically enhanced [26].

TiO_2 has many advantages including high photosensitivity, high structure stability under solar irradiation and in solutions, non-toxic, and low cost. Many applications actually stem from the important feature of the photoassisted catalysis of TiO_2, which is closely related to its surface properties, for example, the bandgap makes it a good absorber of the ultraviolet; in the painting and cosmetic industry TiO_2 is the white color pigment, in the electronic industry, it can be used as gate insulator in the microelectronic devices, and in the architecture, it can be used as a photocatalyst in self-cleaning surfaces by using the superhydrophilicity. As mentioned before, the mesoporous structure of the films is crucial for a high dye loading in the semiconductor. Due to these properties, TiO_2 is the preferred material for DSSC devices.

TiO_2 occurs in three crystal modifications, namely rutile, anatase and brookite. While rutile is the thermodynamically stable phase, anatase is preferred for DSSCs, due to its larger band gap ($E_g \approx 3.2$ eV for anatase compared to $E_g \approx 3.0$ eV for rutile, corresponding to an absorption edge of λ_g ~390 nm and λ_g ~410 nm, respectively) [27]. This leads to a higher Fermi level and open circuit voltage V_{oc} in DSSCs for the same conduction band electron concentration.

2.3.3 Dye as the Photosensitizer

Due to the wide bandgap of TiO_2, it absorbs the photons up to 390 nm. So that in order to harvest as much as possible of the solar spectrum reaching the Earth's surface, dye molecules which chemically bound to the TiO_2 surface acting as antennas. In order to choose a dye molecule there are, a few criteria has to be fulfilled to make sure that the sensitization occurs efficiently.

1. The dye should have a broad absorption spectrum, in order to capture as much as possible of the solar radiation.
2. The extinction coefficient (ε) of the dye should be high over the whole absorption spectrum, to absorb most of the light with a minimum of dye.
3. The excited state of the dye must energetically lie above the conduction band edge of the semiconductor, to guarantee fast electron injection.
4. The excited state lifetime of the dye must be long enough for efficient electron injection.
5. The oxidized dye must have a more positive potential than the redox couple in the electrolyte, in order to prevent recombination of the injected electron with the oxidized dye. On the other hand, the redox potential of the electrolyte should be rather positive, since it determines the potential of the counter electrode and thus the photovoltage of the cell.
6. The dye needs attaching groups (-COOH, $-H_2PO_3$, $-SO_3H$, etc.) to improve the chemical bonding with the semiconductor surface and possibly to work as bridges for electron injection.
7. The dye should be soluble in some solvent for adsorption on the electrode, and

should not be desorbed by the electrolyte redox.

8. The photosensitizer should have chemical, thermal and electrochemical stability during exposure to solar radiation and in the electrolyte media.

2.3.4 The Electrolyte Redox

The electrolyte plays a very important role in the DSSC by facilitating the transport of charge between the working and counter electrodes. The electrolyte function is to regenerate the oxidized dye, and to transfer the positive charge to the counter electrode, where the redox-couple itself is regenerated by an electron flowing back through the external circuit. The electrolyte can be present both in the liquid and solid-state. Nevertheless, some aspects are essential for any electrolyte:

1. The redox couple must have a more negative electrochemical potential than the oxidized dye, so that reduction can take place.
2. On the other hand, the redox potential should be as positive as possible, since the open circuit voltage depends on the potential of the counter electrode and thus the electrolyte.
3. The redox-couple must be reversible at the counter electrode but should not react on the TiO_2 electrode.
4. The electrolyte must not absorb strongly in the visible spectrum.
5. The electrolyte must be able to carry a current of up to $20mA/cm^2$ without diffusion limitation or significant ohmic losses.
6. The electrolyte should have long term chemical, thermal and electrochemical stability.

The most commonly used electrolyte in DSSCs is iodide/triiodide in an organic solvent as acetonitrile (ACN), which also yields the highest efficiency cells [28]. However, it can seriously corrode the TCO-glass resulting in poor long term stability [29, 30].

2.3.5 The Counter Electrode

The counter electrode is another critical component in DSSC where the mediator is reduced. It consists of FTO glass coated with platinum (Pt) to afford more reversible electron transfer. Some of the advantages of Pt are its high catalytic activity towards the iodide/triiodide redox reaction. In order to keep the cell manufacturing costs low, only a few nanometer layer of Pt is needed even if Pt is an expensive element, and because the thin layer of Pt is almost transparent, platinized counter electrodes can be employed also in cells which require reverse lighting. Platinum is also chemically stable in the electrolyte. Other materials like graphite, carbon black, activated carbon on FTO glass and organic-ion doped conducting polymer of poly(3,4-ethylenedioxythiophene) (PEDOT) on both ITO and FTO-glass have been employed as counter electrode in DSSCs [31]. In some cases, a very thin layer of gold could help to improve the fill factor. Recently, however, neither of these materials can achieve the efficiencies obtained with platinum.

The function of the counter electrode is to transfer the electrons arriving from the external circuit back to the redox electrolyte. Hence, it must be well conducting and exhibit a low overvoltage for reduction of the redox couple. In addition, it may serve as mirror, reflecting the light transmitted by the photoelectrode to traverse it a second time, thus enhancing light absorption with a giving amount of dye.

2.4 Operating Principles of Dye Sensitized Solar Cells

The DSSC differs from other solar cell types both by its basic construction and the physical processes behind its operation. Unlike the 1st and 2nd generations of PV devices based on solid semiconductor materials, the typical DSSC configuration combines solid and liquid phases. The main difference to Si-based solar cells lies in the separation between charge generation (dye molecule) and charge-transport (TiO_2) and the fact that charge separation occurs by means of kinetic irreversibility rather than by a built-in electrical field. Furthermore, the initial photoexcited species in organic molecules are different from those of silicon.

Generally, the key processes in the operating mechanism of a DSSC can be divided into four basic steps

1. Light absorption
2. Charge separation
3. Charge collection
4. Dye regeneration

The efficiency of the DSSC depends on the optimization of each of the interfacial electron transfer processes.

The principle of operation of a DSSC is quite simple, shown by the scheme in Fig. 2.2. The crucial idea is to separate the light absorption process from the charge collection process, mimicking natural light harvesting procedures in photosynthesis, by combining dye sensitizers with semiconductors.

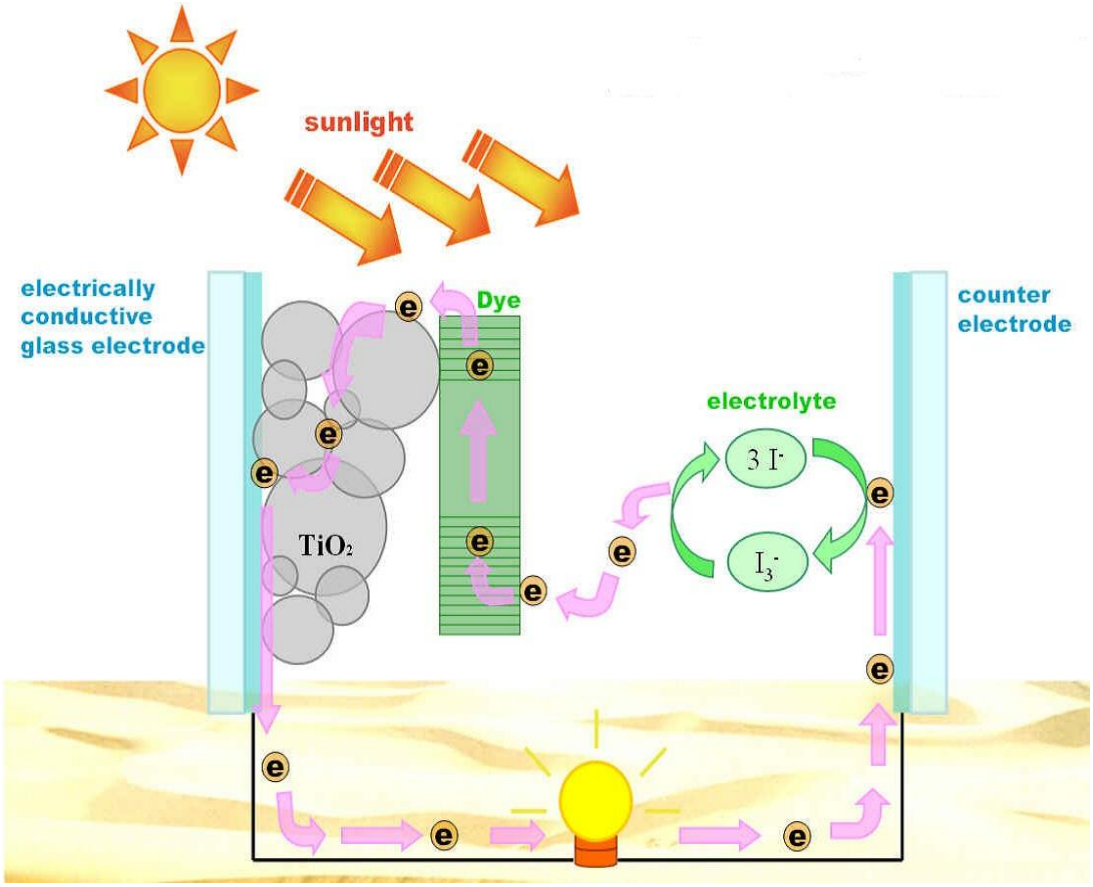

Fig. 2.2 Operation scheme of a dye sensitized solar cell [32].

The processes happening during cell's operation are presented in Fig. 2.2 and they are briefly described below.

2.4.1 Light Absorption and Electron Injection

Photons of different energies in the sunlight strike the cell, penetrating into the dye layer due to the transparency of both the FTO layer with glass substrate and the TiO_2 nanoparticles to visible light. If photon energy is close to the energy gap of the dye molecule, namely, the energy difference between the highest occupied molecular orbital (HOMO) and lowest unoccupied molecular orbital (LUMO), it will be absorbed by the dye, promoting one

electron from HOMO to LUMO. This excited electron can be injected from the excited state of the dye molecule into the conduction band of the semiconductor TiO_2 through the interfacial bonds between the dye and the TiO_2. This process of the electron injection, which given by equation 2.2, is one of the fastest known physical phenomena [33] and it occurs on the femtosecond scale. This is a crucial step, because this is the moment when the charge separation takes place.

2.4.2 Electron Transport and Collection

In order to generate electrical energy, photo-injected electrons in the conduction band of the semiconductor should be transported through the mesoporous network by diffusion reaching the FTO. The electrons reach the counter electrode through the external load. The time scale at which the transport occurs is in the ms range.

2.4.3 Dye Regeneration

After the electron injection the dye molecule becomes oxidized, therefore it has to be consequently reduced to ensure the continuous operation of the device. This is done by the reduced form of the redox mediator present in the electrolyte. Therefore, the oxidized dye molecules are regenerated by receiving electrons from the I^- ion redox mediator that became oxidized to I_3^- (Tri-iodide ions). For efficient operating of DSSC, the oxidized dye should be reduced to its original state after the electron injection as fast as possible. The oxidized form of the redox mediator I_3^- needs to be reduced and this takes place at the counter electrode, which substitutes the internally donated electron with that from the external load and reduced back to I^- ion. Therefore, from this cycle, generation of electric power in DSSC causes no

permanent chemical change or transformation [34].

The operating cycle of DSSC can be summarized in the following chemical reactions

Anode:	$S + \mathrm{h}v \longrightarrow S^*$	Photo-excitation of the dye	(2.1)
	$S^* \longrightarrow S^+ + e^- (TiO_2)$	Electron injection in TiO_2	(2.2)
	$2S^+ + 3I^- \longrightarrow 2S + I_3^-$	Regeneration of the dye	(2.3)
Cathode:	$I_3^- + 2e^-(Pt) \longrightarrow 3I^-$	Reduction of the redox	(2.4)

The main loss processes in a DSSC are:

1. The relaxation of the excited electron back to the ground state of the dye.
2. The recombination of the injected electron with the oxidized dye.
3. The loss of the injected electron in the conduction band to the triiodide in the electrolyte (also known as the dark current).

The efficiency of charge separation and energy conversion depends on the kinetic competition between the various forward steps and the charge-recombination processes.

2.5 Key Efficiency Parameters of DSSC

The performance of the DSSC is mainly characterized by the following parameters such as incident photon to current efficiency (IPCE), short circuit photocurrent density (J_{sc}), open circuit photovoltage (V_{oc}), the fill factor (FF) and the overall efficiency of the photovoltaic cell (η).

2.5.1 Incident Photon to Current Conversion Efficiency (IPCE)

The spectral response of the dye sensitized solar cell depends on the absorption properties of

the dye. The incident photon to current conversion efficiency (IPCE), also known as an external quantum efficiency (EQE), is one of the key parameters of quantitative characterization of the solar cell performance for the fact that IPCE shows the spectral response of solar cells to various incident wavelengths. It measures how efficiently the incident light of a specific wavelength is converted into electron/hole pairs, by measuring the ratio between the number of electrons generated by the solar cell and collected at the external circuit and the number of photons of a given wavelength shining on the solar cell [35,36]. The IPCE can be calculated according to equation.

$$IPCE = \frac{1240.J_{sc}}{\lambda.P_{in}} \tag{2.5}$$

where J_{sc} is the short circuit photocurrent density (mA/cm^2), λ is the wavelength (nm), P_{in} is incident power (mW/cm^2).

2.5.2 Short Circuit Photocurrent Density (J_{sc})

J_{sc} is the photocurrent per unit area (mA/cm^2) when an illuminated cell is short circuited where the external output voltage is zero. It depends on several factors such as the light intensity, light absorption, injection efficiency, regeneration of the oxidized dye, and the efficiency of charge transport in the TiO_2 film to the counter electrode. It is strongly related to the IPCE and theoretical values of the J_{sc} can be calculated from integrated sum of IPCE measure over the entire solar spectrum**.**

$$I_{sc} = \int_0^{\infty} IPCE(\lambda).I_{sun}(\lambda)d\lambda \tag{2.6}$$

2.5.3 Open Circuit Photovoltage (V_{oc})

V_{oc} is measured when the circuit is open or no external load is connected. Under this

condition, there is no external current flows between the two terminals i.e. I = 0 and V = V_{oc}. It depends on both the Fermi level of the semiconductor and the level of dark current. The theoretical maximum of the V_{oc} of the cell is determined by the difference between the Fermi level of the semiconductor and the redox potential of the electrolyte.

2.5.4 Optimum Voltage (V_m)

V_m is the voltage at the optimum operating point at which the DSSC output power is maximum.

2.5.5 Optimum Current (I_m)

The value of I_m gives the maximum photocurrent obtainable at maximum power point.

2.5.6 Output Power (P_{out})

For a given bias voltage the output power of the cell is the product of the measured current density and the bias voltage

$$P_{out} = V.J \tag{2.7}$$

P_{out} generally increases when V is increased from zero, goes through a maximum and decreases to zero at V = V_{oc}. The maximum power point P_m is the product of I_m and V_m which corresponds visually to the area of the largest rectangle as shown in Fig. 2.3.

2.5.7 Fill Factor (FF)

Fill factor is a parameter related to the maximum power point and is often described as a measure of the "squareness" of the J-V curve and describes the degree to which the voltage

at the maximum power point (V_m) matches V_{oc} and that the current at the maximum power point (I_m) matches I_{sc}. Fill factor is the ratio of the areas of two rectangles under the IV curve as shown in Fig. 2.3. Moreover, its value is determined by the ratio of the maximum power (V_mI_m) to the maximum power attainable by the solar cell ($I_{sc}V_{oc}$), with a value between 0 and 1.

$$FF = \frac{V_m I_m}{I_{sc} V_{oc}} \tag{2.8}$$

2.5.8 Solar Energy to Electricity Conversion Efficiency (η)

The overall solar energy to electric power conversion efficiency (η), the key parameter of the device, measures how much power is converted by the cell in comparison to the amount of absorbed light that reaches the device. It is given by the ratio of the maximum output power (V_mI_m) to the incident solar power (P_{in}). The overall sunlight to electric power conversion efficiency of a DSSC is given by the following expression

$$\eta = \frac{P_m}{P_{in}} = \frac{J_{sc} V_{oc} FF}{P_{in}} \tag{2.9}$$

2.5.9 Standard Measurements

The efficiency of a solar cell is highly depending on the incident irradiation, so in order to compare the results of different research groups, a standard measurement condition is needed. The standard test condition for solar cells is the Air Mass 1.5 G solar spectrum, an incident power density of 1000 W/m^2 (100 mW/cm^2), and temperature of the cell is 25°C.

A typical I-V curve of a solar cell is shown in Fig. 2.3. By convention, the applied bias voltage is positive, and the measured solar cell current is negative.

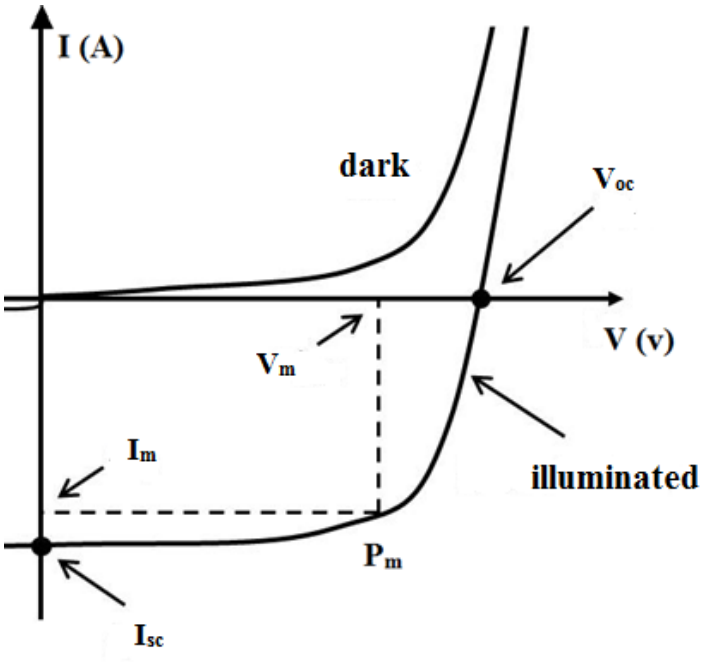

Fig. 2.3 Typical I-V curve of a solar cell showing the open circuit voltage V_{oc}, short circuit current I_{sc}, and the maximum power point P_m.

2.6 Electrochemical Impedance Spectroscopy

The IV-curve measurements give only quite superficial information about the cell operation for instance, they do not directly tell the physical reasons why a cell works efficiently or not. One way, to obtain a better understanding of the processes that play a role in the cell behavior, is by modeling the device with an equivalent electrical circuit comprising different electrical components. Those different electrical components can be related to chemical or physical processes that occur in the device. Therefore, finding a suitable equivalent circuit will help understanding the behavior of the device. Impedance spectroscopy is the most common tool to obtain the equivalent circuit.

The meaning of electrical impedance can be understood from the concept of resistance. The electrical resistance is the ability of a circuit element to resist the flow of electrical current. The well-known Ohm's law defines the resistance (R) in terms of the ratio between voltage

(V) and current (I).

$$R = \frac{V}{I} \tag{2.10}$$

This relationship is limited to only one circuit element, an ideal resistor. But usually the systems under study contain circuit elements that exhibit a much more complex behavior. The simple concept of resistance needs to be replaced by a more general parameter; the impedance, which includes not only the relative amplitudes of the voltage and the current (equation 2.10), but also the relative phases. Like resistance, impedance is a measure of the ability of a circuit to resist the flow of electrical current [37].

The most common and standard procedure in impedance measurements consists of applying a small voltage sinusoidal perturbation and observing the resulting current response of the system at the corresponding frequency.

Based on the definition of resistance described by Ohm's law, the current voltage relationship in impedance can be expressed as

$$Z(\omega) = \frac{V(t)}{I(t)} \tag{2.11}$$

where V(t) and I(t) are measurements of voltage and current in an AC system and ω is the frequency of the AC signal.

For a sinusoidal system, the AC impedance of a resistor Z_R, can be expressed as

$$Z_R = R \tag{2.12}$$

The AC impedance of a capacitor Z_C, can be expressed as

$$Z_c = \frac{1}{i\omega c} \tag{2.13}$$

And the AC impedance of an inductor Z_L, can be expressed as

$$Z_L = i\omega L \tag{2.14}$$

The impedance of an electrochemical system can also be expressed typically in cartesian

coordinates:

$$Z(\omega) = Z' + iZ'' \tag{2.15}$$

where Z' or Z_{Re} and Z" or Z_{im} are the real and imaginary parts of Z, respectively, and $i = \sqrt{-1}$.

2.7 Nyquist Plot

One of the representations of the impedance spectrum of an electrochemical system is a Nyquist plot which displays $-Z_{im}$ vs Z_{Re} for different values of ω as shown in Fig. 2.4.

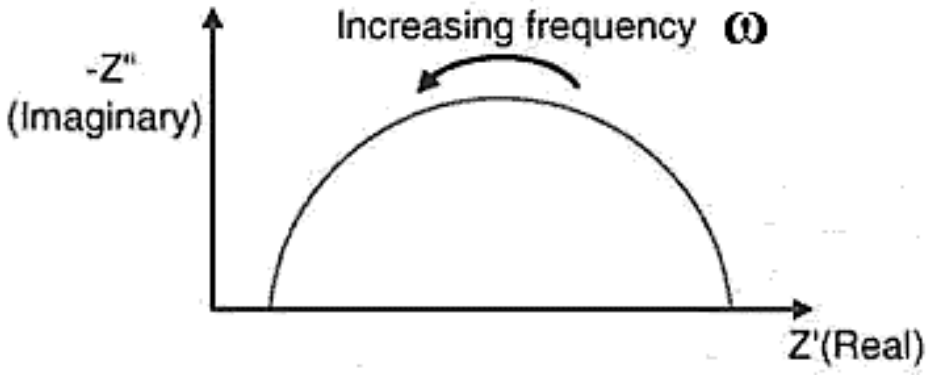

Fig. 2.4 A Nyquist plot (complex-plane diagram).

2.8 Bode Plot

As discussed before, impedance spectra are often represented in complex impedance-plane or Nyquist plots accompanied with Bode representations in which the phase angle is presented as a function of frequency. Such Bode plot of impedance data is given in Fig. 2.5.

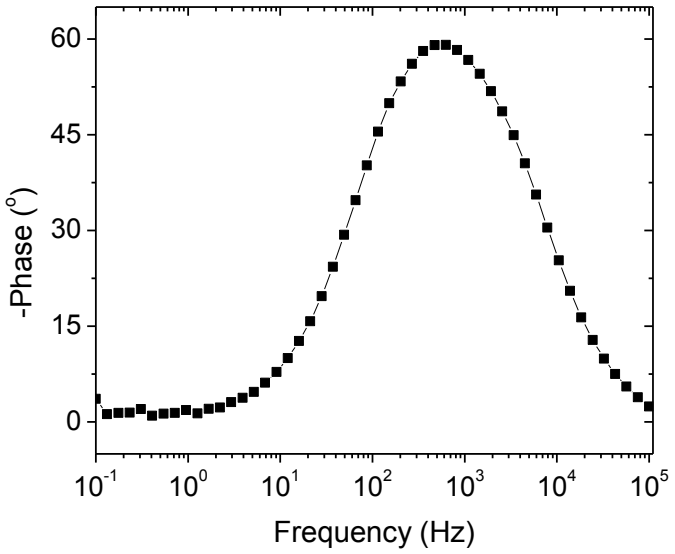

Fig. 2.5 Bode plot showing the phase angle as a function of frecuency.

2.9 Equivalent Circuits

One of the most attractive aspects of impedance spectroscopy is the direct connection that often exists between the behavior of a real system and that of an idealized model circuit consisting of discrete electrical components. The first step in developing an equivalent electrical circuit for an electrochemical system is to analyze the nature of the overall current and potential.

In general a solar cell can be perceived as a current source (I_{photo}) connected with a diode(s) in parallel (I_{01} and I_{02}), but due to its non-ideality, a shunt resistance (R_{shunt}) is also a part of an equivalent circuit as shown in Fig. 2.6 [38].

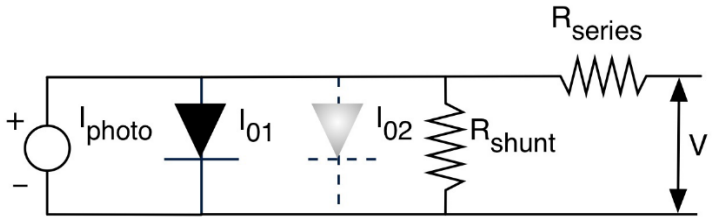

Fig. 2.6 The equivalent circuit of a solar cell.

The shunt current (I_{shunt}) is induced by the charge recombination processes. Series resistance (R_{series}) is an element that groups together the contact resistances at the interfaces, the bulk resistance and the sheet resistances of the transparent glass supports.

CHPTER THREE

3. RESEARCH TECHNIQUES

3.1 Experimental Techniques

A brief description is given for the experimental techniques used to synthesize and characterize DSSCs. The experimental procedure is described as well. The method of examining the optical properties of the dye using ultraviolet–visible (UV-Vis) spectroscopy is presented. Voltage-current characteristics and the cell performance can be obtained with a solar simulation which is presented here. Moreover, impedance spectroscopy is also described.

Finally, the materials and techniques used for the preparation of DSSC are discussed.

3.1.1 UV-Vis Spectroscopy

Ultraviolet and visible (UV-Vis) absorption spectroscopy is the measurement of the attenuation of a beam of light after it passes through a sample or after reflection from a sample surface. Absorption measurements can be at a single wavelength or over an extended spectral range. The basic parts of the spectrophotometer are light source, monochromator with diffraction grating to separate the different wavelengths of light, sample holder and detector as shown in Fig. 3.1.

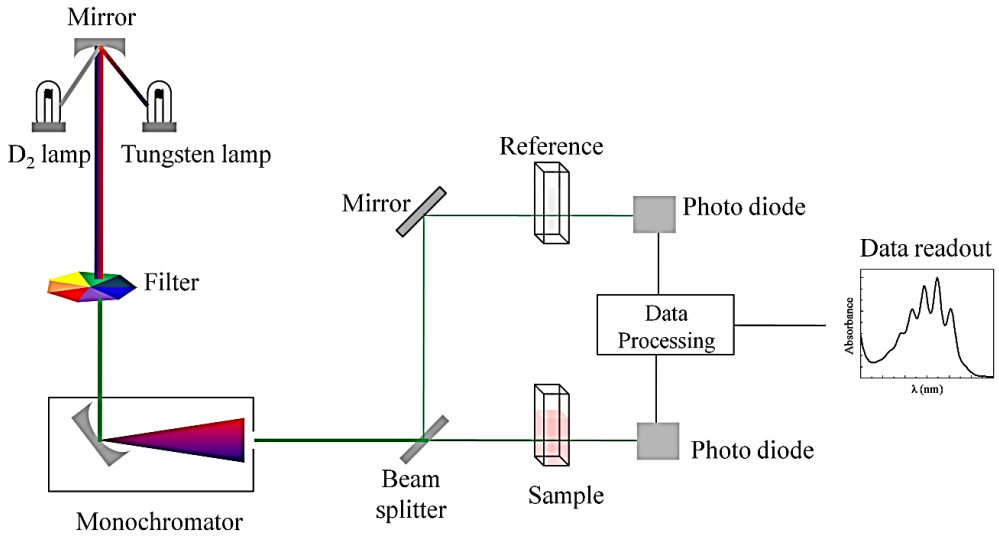

Fig. 3.1 Schematic representation of UV-visible spectrophotometer [39].

The UV-Vis spectral range is approximately 190 to 900 nm, as defined by the working range of typical commercial UV-Vis spectrophotometers [40]. The ultraviolet (UV) region scanned is normally from 200 to 400 nm, and the visible portion is from 400 to 700 nm.

The functioning of this instrument is relatively straightforward. A beam of light from a visible or UV light source is separated into its component wavelengths by a prism or diffraction grating. Each monochromatic (single wavelength) beam in turn is split into two equal intensity beams by a half-mirrored device. One beam, the sample beam, passes through a small transparent container (cuvette) containing a solution of the compound being studied in a transparent solvent. The other beam, the reference, passes through an identical cuvette containing only the solvent. The intensities of these light beams are then measured by electronic detectors and compared. The intensity of the reference beam, which should have suffered little or no light absorption, is defined as I_0. The intensity of the sample beam is defined as I. Over a short period of time, the spectrometer automatically scans all the component wavelengths in the manner described.

To obtain the ratio I / I_0 which does not depend on changes of the incident light intensity and is called the transmittance

$$T = I/I_0 \tag{3.1}$$

The absorption coefficient α for a uniform medium can be defined in terms of the intensity change of a monochromatic light beam in a unit distance that the beam travelled in the medium by [41]

$$\frac{dI}{dx} = -\alpha I \tag{3.2}$$

Therefore, the beam intensity as a function of the distance x can be written as

$$I = I_0 e^{-\alpha x} \tag{3.3}$$

The absorbance (A) is defined as follows

$$A = -\log T \tag{3.4}$$

Absorption may be presented as transmittance (T) or absorbance (A). If no absorption has occurred, T = 1 and A= 0.

It is therefore clear that the absorbance and absorption coefficient are proportional to one another.

If the sample compound does not absorb light of a given wavelength, $I = I_0$. However, if the sample compound absorbs light then I is less than I_0, and this difference may be plotted on a graph versus wavelength as shown in Fig. 3.2. The wavelength of maximum absorbance is a characteristic value, labelled as λ_{max}.

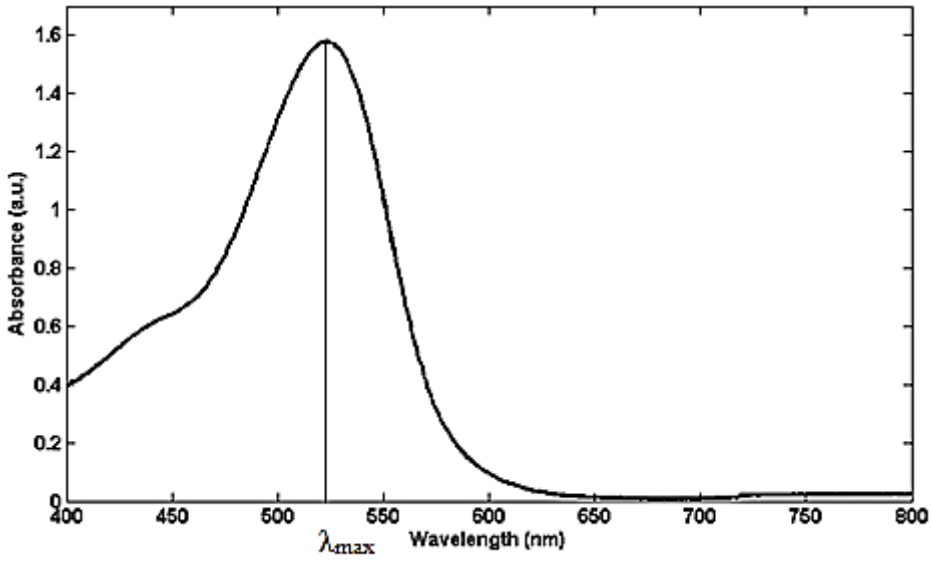

Fig. 3.2 Absorption of light by dye using UV-Vis spectroscopy.

Our absorption spectra were recorded by GENESYS 10S UV-Vis spectrophotometer. The UV-Vis spectroscopy used in this study is shown in Fig. 3.3.

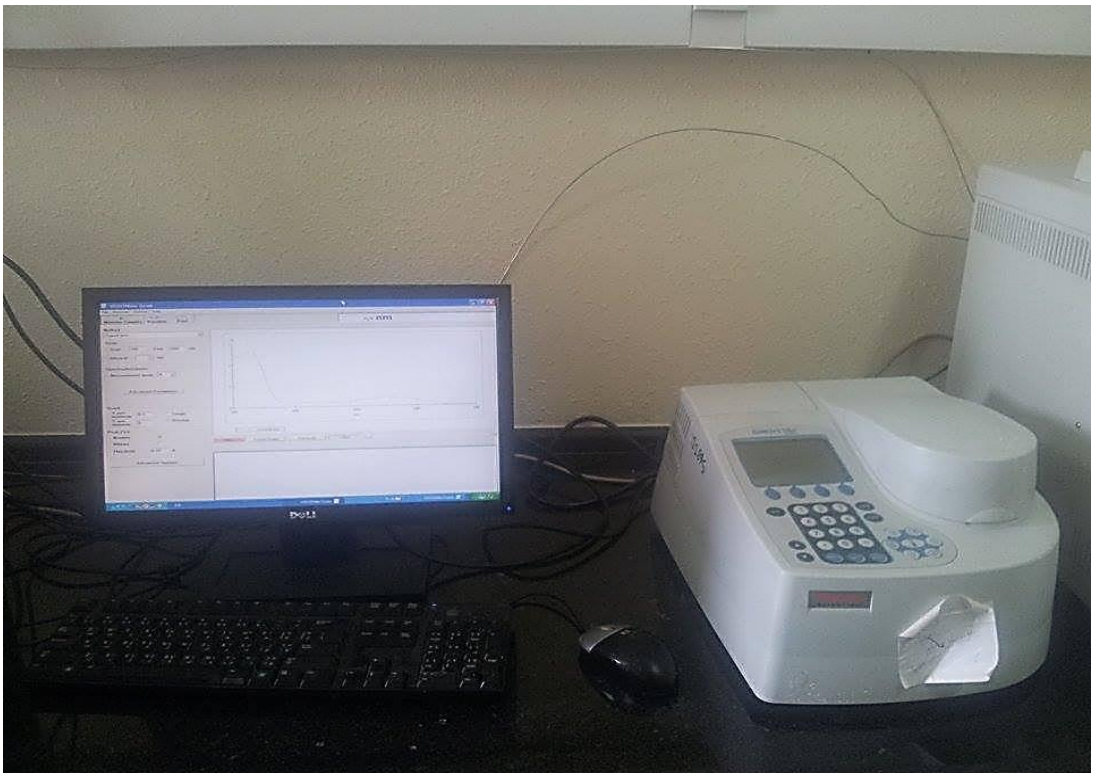

Fig. 3.3 GENESYS 10S UV-Vis spectrophotometer.

3.1.2 Solar Cell I-V Measurement Systems

Because solar radiation is not always available and its magnitude differs according to location and surroundings, a solar simulation is used in solar cell performance measurements. This system includes a light source, measurement electronics, computer, and software needed to measure solar cell I-V curves. The illuminated current versus voltage (I-V) characteristics of a photovoltaic (PV) device typically measured with respect to standard reference conditions, are defined by a spectrum, intensity, temperature and area. Our target is to create a light source which can simulate the solar standard AM1.5 as closely as possible for testing our solar cells using inexpensive components.

Once the solar simulator intensity has been set to match the standard intensity and spectrum using a reference cell for the particular device being evaluated the I-V characteristics can be measured using Labview Program. The Labview software is applied in this work to pack and draw the collected data of solar cell characteristics from microcontroller subsystem. A J-V measurement system measures J-V curves of solar cells and calculates critical cell performance parameters including short circuit current (I_{sc}), open circuit voltage (V_{oc}), fill factor (FF), maximum current (I_{max}), maximum voltage (V_{max}), maximum power (P_{max}), and efficiency (η) and saves test data in text files for using it to characterize the cell.

A voltage in the range -1 to 1 is applied to the solar cell and the resulting current is measured using NI USB6251 data acquisition card in combination of a Labview program. Photovoltaic tests of the fabricated DSSCs using natural dyes as sensitizers were performed by measuring the J–V curve of each cell under irradiation with white light (100mW/cm^2) from a tungsten halogen lamp with blue filter as shown in Fig. 3.4.

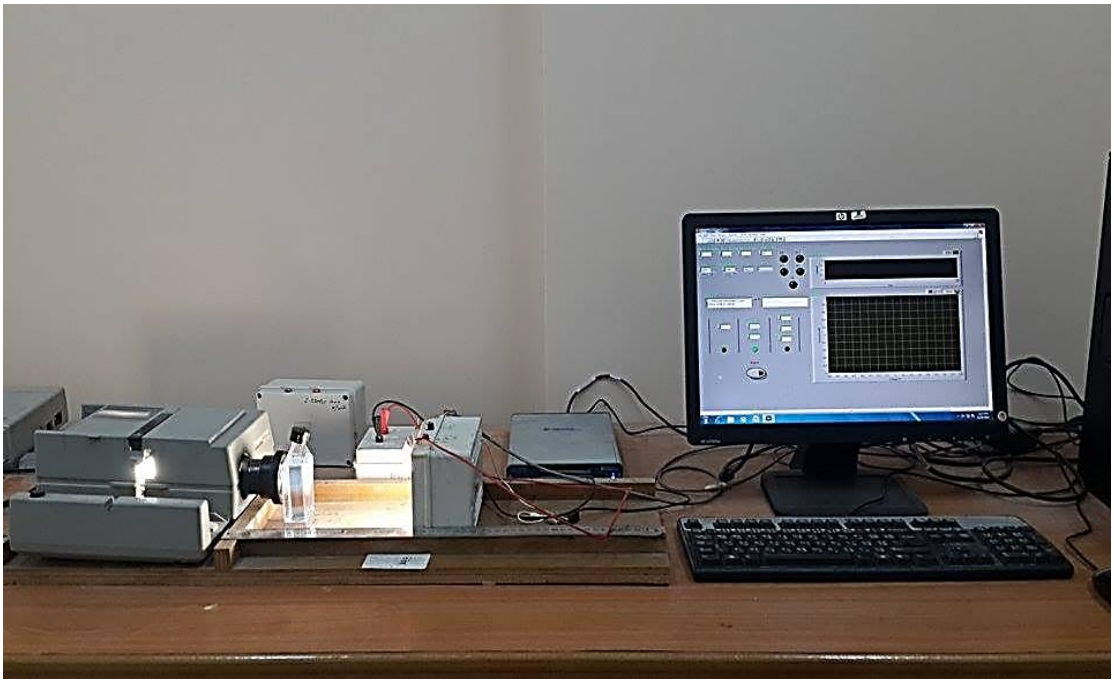

Fig. 3.4 Solar cell simulator and I-V measurement systems.

3.1.3 Electrochemical Impedance Spectroscopy (EIS)

In recent decades, research has intensified to develop commercially viable solar cells as a clean and efficient source of energy, due to the global shortage of fossil fuels. The challenge is to achieve a cell lifetime suitable for transportation and stationary applications. EIS has also proven to be a powerful technique for studying the fundamental components and processes in solar cells, and is now widely applied to the study of DSSCs as well.

Our EIS measurements were performed by Autolab AUT 85276 Potentiostat- Gelvanostat with frequency response analyzer FRA 32 Module as shown in Fig 3.5.

In a typical electrochemical impedance measurement, the FRA module generates a sine wave with a user-defined frequency and small amplitude. This signal is superimposed on the applied DC potential or current on the device. The total impedance Z, is calculated together with the phase angle shift and the real and imaginary components of the total

impedance. The AC amplitude of voltages were set to -0.4 v,-0.6 v and -0.8 v under dark and illuminated conditions for all measurements, all the measurements were carried out with the NOVA software. The impedance was measured and plotted to obtain Nyquist plot.

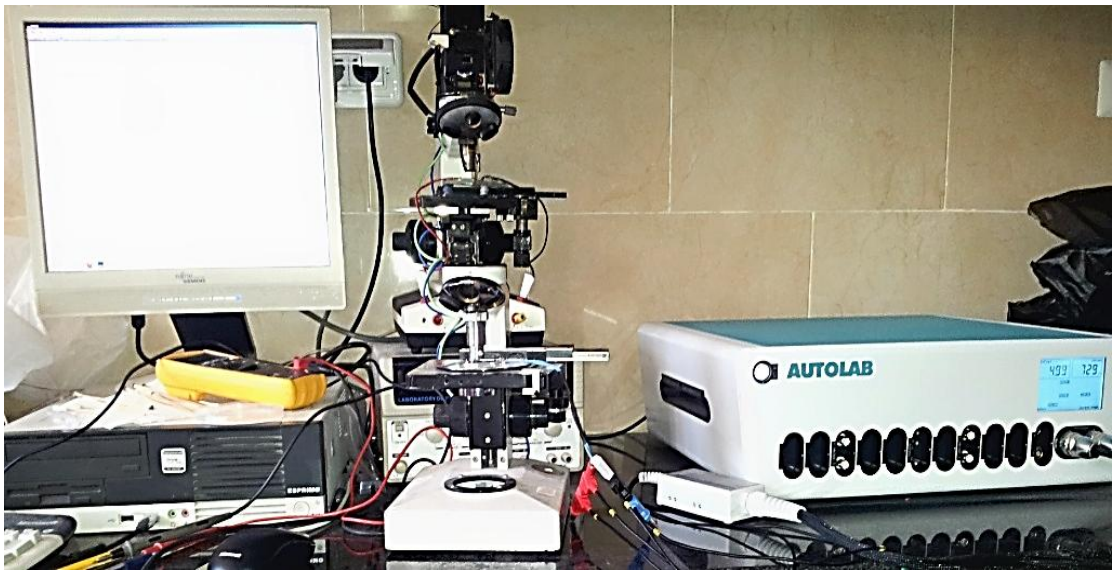

Fig. 3.5 Autolab AUT 85276 Potentiostat- Gelvanostat with frequency response analyzer FRA 32 Module.

Any electrochemical interface (or cell) can be described in terms of an electric circuit, which is a combination of resistances, capacitances, and complex impedances (and inductances, in the case of very high frequencies). If such an electric circuit produces the same response as the electrochemical interface (or cell) does when the same excitation signal is imposed, it is called the equivalent electric circuit of the electrochemical interface (or cell). The equivalent circuit should be as simple as possible to represent the system targeted. Electrochemical Impedance Spectroscopy can establish a hypothesis using equivalent circuit models. A data-fitted equivalent circuit model will suggest valuable chemical processes or mechanisms for the electrochemical system being studied.

3.2 Device Fabrication

In this section, DSSCs prepared using natural dyes extracted from plant roots as photosensitizers are described.

3.2.1 Materials Used in Preparing of DSSCs

a. Fluorine-doped SnO_2, conductive plates with sheet resistance 15 Ω/□, and transmission >80% (Xinyan Tech. Ltd, Hong Kong).
b. TiO_2 nanoparticles with 10-25 nm (US Research Nanomaterial, Lnc, USA).
c. Natural dyes extracted from plant roots listed in Table 3.1.
d. A counter electrode fabricated from FTO-coated glass, with sputtered platinum catalyst layer.
e. A redox (I^-/I_3^-) electrolyte solution.
f. Electrical contact between working and counter electrodes is achieved using alligator clips.

3.2.2 Extraction of the Natural Dyes

Six plant roots were collected from various plants. The collected roots were thoroughly washed with water to remove the adhering particles and dust from the surface. The roots were then dried in a refrigerator for 24 hours. One gram of the roots were immersed in 10ml of Ethanol at room temperature and kept in the dark for one day. After filtration of the solutions, natural extracts were obtained. The natural roots used in this study are listed and shown in Table 3.1 and Fig. 3.6.

Table 3.1 Natural roots used in this study.

Dye Code	Name of the root
ND.1	Purple Carrot
ND.2	Carrot
ND.3	Beet
ND.4	Curcuma
ND.5	Kale
ND.6	Radish

Fig. 3.6 The natural roots used in this thesis.

3.2.3 Preparation of the FTO Glass

The FTO conductive glass substrates were cut into pieces of dimensions 1.6 cm×1.6 cm. The glass was cleaned in a detergent solution using an ultrasonic bath for 20 min, rinsed with water and ethanol, and then dried in an oven at 60°C for 30 min. The sheet resistance

of the FTO conductive glass was measured and found to be 15-20 Ω/□.

3.2.4 Preparation of TiO_2 Electrode (Photoanode)

The photoanode is prepared by adsorbing a dye on a porous titanium dioxide, TiO_2 layer deposited on FTO conducting glass. By this approach, the dye extends the spectral sensitivity of the photoanode, enabling the collection of lower energy photons. The semiconductor paste was prepared by blending 2 g of TiO_2 nanopowder, 4 ml distilled water, 10 µl of acetylacetone, and 50 µl of Triton X-100 as the surfactant [42].

Two edges of the FTO glass plate were covered with a layer of adhesive tape as shown in Fig. 3.7 to control the thickness of the film and to mask electric contact strips. Successively the TiO_2 paste was spread uniformly on the substrate by sliding a metallic rod along the tape spacer by doctor-blade technique in order to obtain a TiO_2 layer of 0.25 cm^2 area.

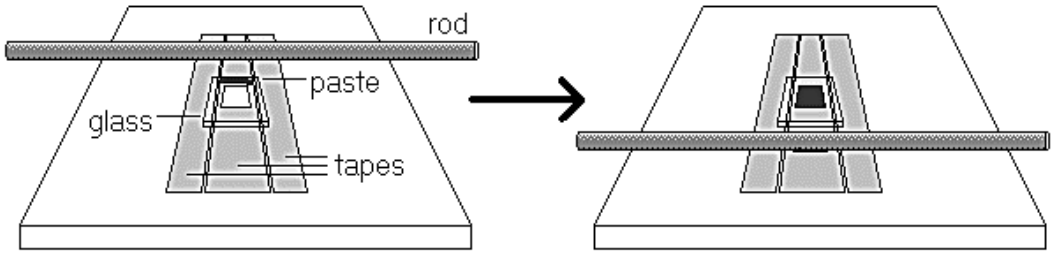

Fig. 3.7 Doctor blade method to spread the TiO_2 paste on the FTO coated glass [43].

After heating up the FTO glass with TiO_2 film to 450°C for about half an hour, the sintering process was completed and the TiO_2 deposited- electrode was cooled down to 100°C. After cooling down to 100°C, the samples were immersed in the natural extracts for 24 h. The thickness of the resulting mesoscopic oxide film was measured using BX 53 Olympus polarizing microscope equipped with DP 73 camera and it was about 20 µm as shown in

Fig. 3.8.

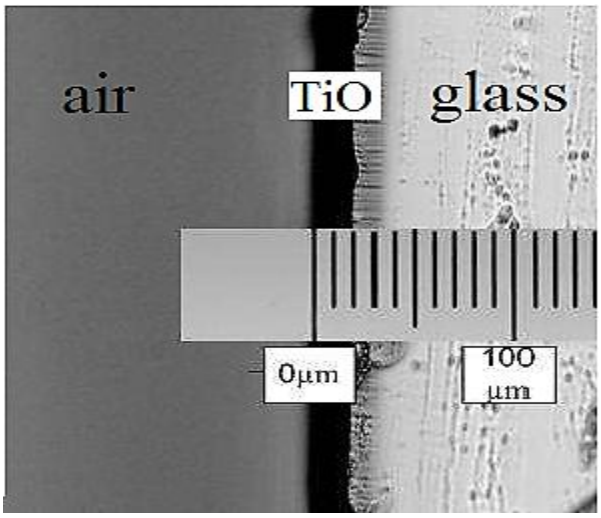

Fig. 3.8 A side of the TiO_2 film under magnification of 100x.

3.2.5 Assembly of DSSC

Finishing fabrication of all parts, the DSSCs were assembled by fixing the dyed TiO_2 electrode and the Pt counter electrode so that the dyed TiO_2 plates facing down onto the coated Pt counter electrode. They should be placed so that they are slightly offset to allow connections (for the crocodile clips). The two electrodes were pressed and clamped firmly in a sandwich configuration. The electrolyte redox (I^-/I_3^-) is spread within the vicinity between the two electrodes using micropipette. Finally, the fabricated DSSC is connected to the solar cell I-V measurement systems and EIS devices mentioned in sections 3.1.2 and 3.1.3, respectively.

CHAPTER FOUR

4. EXPERIMENTAL WORK WITH RESULTS AND DISCUSSIONS

4.1 Introduction

In this chapter, five experimental studies will be discussed in details, including determination of the best dye from six natural dyes extracted from plant roots, optimizing extracting temperature, influence of pH solution of the dye on the DSSC efficiency, pre-treatment of the FTO glass using several acids, and post-treatment of TiO_2 layer .

For the best dye, the absorption spectra, the J-V characteristic curves, the J_{sc}, the V_{oc}, the P_{out}, the FF, and power conversion efficiency η will be presented.

Finally, the electrochemical impedance spectroscopy will be performed for three studies using AUT 85276 Potentiostat- Galvanostat with frequency response analyzer FRA 32 Module device mentioned before in the previous chapter.

4.2 Thesis Statement

4.2.1 Dye Testing

The performance of the DSSC is critically dependent on the type of the dye used as a sensitizer. Many metal complexes and organic dyes have been synthesized and used as sensitizers. Ruthenium (Ru) complexes are considered good sensitizers for DSSCs because of their intense charge-transfer absorption over the entire visible range and highly efficient metal-to-ligand charge transfer [44]. The main disadvantages of Ru are its rarity, high cost and the complicated synthesis of ruthenium complexes. This has led to a great research interest in finding alternative, readily available and efficient photosensitizers at low cost.

Recently, research has focused on the easily available dyes extracted from natural sources as photosensitizers because of large absorption coefficients, high light-harvesting efficiency, low cost, easy preparation and environment friendliness.

The six natural roots purple carrot, carrot, beet, curcuma, kale and radish have been used as sensitizers in DSSCs.

4.2.1.1 Experiment

Six dyes obtained from plant roots of purple carrot, carrot, beet, curcuma, kale and radish were tested as photosensitizers in this work. These dyes were prepared by immersing 1 g of the dried natural roots in 10 ml of ethanol as a solvent for 24 h. All solutions were protected from direct light exposure. After filtration of the solutions, natural extracts were obtained. The TiO_2 electrodes were immersed in these dyes and the fabricated DSSCs were conducted to the solar cell I-V measurement system shown in Fig. 3.4.

4.2.1.2 Results and Discussions

- **Absorption Spectra of Natural Root Extracts**

The Absorption spectra of the dye solutions extracted from the roots of purple carrot, beet and curcuma in ethanol as a solvent in comparison with the Ru (N719) were investigated using GENESYS 10S UV-Vis spectrophotometer available at the Islamic university of Gaza (IUG), Gaza-Palestine. The absorption spectra analysis was carried out in the wavelength range from 390 to 700 nm as shown in Fig. 4.1.

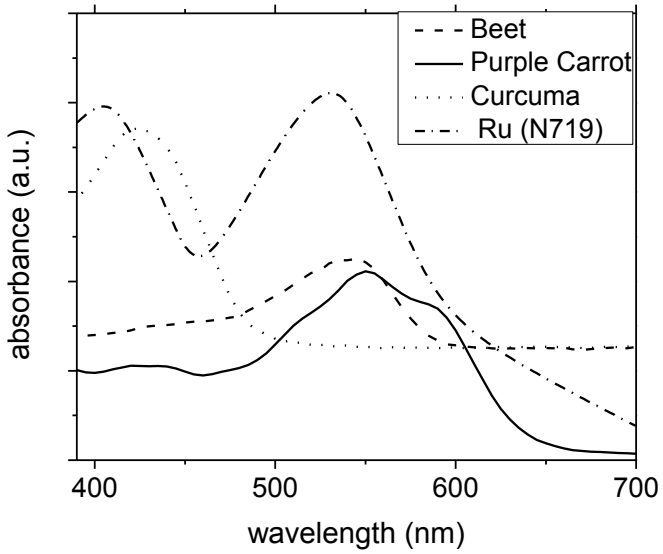

Fig. 4.1 The UV–Vis absorption spectra of beet, purple carrot, curcuma and Ru (N719).

As observed from Fig. 4.1, the absorption peaks are found at 427 nm and at 552 nm for purple carrot, for beet at 544 nm, for curcuma at 424 nm, whereas for Ru (N719) there are two peaks at 408 nm and at 528 nm. Generally, it is found that the dye extracted from purple carrot has a wide band with absorption peaks at about 550 nm and 427 nm. This is due to that the existing anthocyanin pigment [45].

❖ J-V Characterization of DSSCs Sensitized with the Extracts of Natural Roots

Once the DSSC is fabricated, it is now important to evaluate its performance. The J-V characteristic curves of the DSSCs sensitized with the extracts of purple carrot, carrot, beet, curcuma, kale and radish are shown in Fig. 4.2.

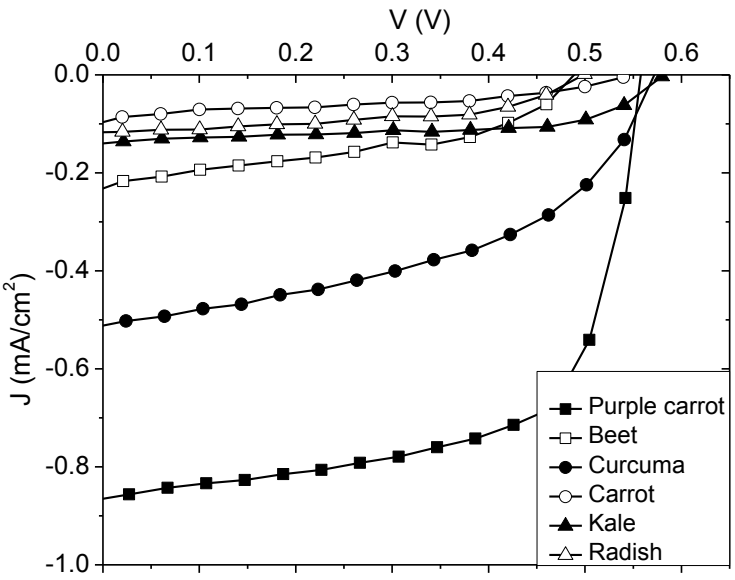

Fig. 4.2 Current density (J) versus voltage (V) characteristic curves for the DSSCs sensitized by the extracts of purple carrot, carrot, beet, curcuma, kale and radish.

As shown in Fig. 4.2 the values of J_{sc} and V_{oc} can be obtained for all DSSCs directly using the J- V data. The power is calculated according to equation 2.7 and plotted versus the voltage for all DSSCs at that intensity as shown in Fig. 4.3. The maximum power point is determined from the power (P)-voltage (V) curves from which J_m and V_m can be obtained. The fill factor and cell efficiency are calculated using equation 2.8 and equation 2.9, respectively. All the photovoltaic parameters of the fabricated DSSCs sensitized by purple carrot, beet, curcuma, carrot, kale, and radish are listed in Table 4.1.

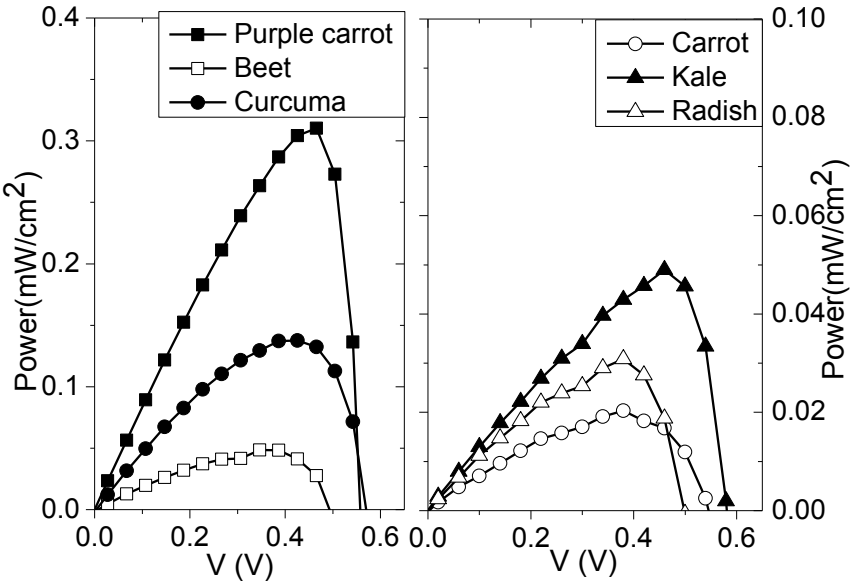

Fig. 4.3 Power (P) versus voltage (V) characteristic curves of the fabricated DSSCs.

Table 4.1 Photovoltaic parameters of the DSSCs sensitized by natural dyes extracted from plant roots.

Dye	J_{sc} (mA/cm^2)	V_{oc} (V)	J_m (mA/cm^2)	V_m (V)	FF	η %
Purple carrot	0.87	0.56	0.69	0.46	0.66	0.32
Curcuma	0.51	0.57	0.33	0.42	0.47	0.14
Beet	0.23	0.49	0.14	0.36	0.43	0.05
Carrot	0.10	0.55	0.06	0.38	0.42	0.02
Kale	0.14	0.58	0.11	0.46	0.56	0.05
Radish	0.12	0.50	0.08	0.38	0.55	0.03
Ru (N719)	4.76	0.57	3.53	0.38	0.50	1.35

Giving the data present in Table 4.1, the J_{sc} has a maximum value of 0.87 mA/cm^2 for the DSSC sensitized with the dye extracted from purple carrot, and a minimum value of 0.10 mA/cm^2 for the DSSC sensitized with the dye extracted from carrot. The V_{oc} ranges between 0.49 V for DSSCs sensitized with beet extract and 0.58 V for the cell dyed with kale. The fill factor of the fabricated cells changes from 41.5% to 65.7%. The highest fill factor was obtained for the DSSC sensitized with the extract of purple carrot and the lowest fill factor was observed for the cell dyed with carrot. The highest output power and efficiency were obtained for the DSSC sensitized with purple carrot where the efficiency of the cell reached 0.32%, while the lowest efficiency was obtained for the DSSC sensitized with carrot where it reached 0.02%. Based on Table 4.1, purple carrot showed the best efficiency. Therefore it was chosen as a sensitizer for further studies.

Good photo-to-electric conversion ability in a DSSC is strongly dependent on available chemical bonds between the dye molecules and TiO_2 particles, through which electrons can transport from excited dye molecules to the TiO_2 film. Dye extracted from purple carrot, which contains anthocyanin is a class of pigments found in many berries and other plants and they appear red, blue or purple depending on pH. The advantage of anthocyanin is the binding of carbonyl and hydroxyl groups to the surface of a porous TiO_2 film as shown in Fig 4.4. This causes electron transfer from the anthocyanin molecule to the conduction band of TiO_2.

Anthocyanin extracts have been studied as sensitizers for DSSCs application [46]. Moreover, anthocyanin from various plants gave different levels of sensitizing performance [47-48].

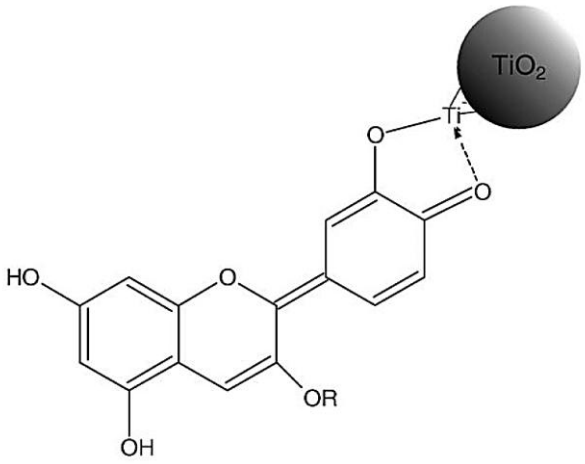

Fig. 4.4 The basic molecular structure of anthocyanin and the binding between anthocyanin molecule and TiO_2 particles [44].

Diffuse reflectance spectra were collected with a V-670, JASCO spectrophotometer and transformed to the absorption spectra according to the Kubelka-Munk relationship.

Figure 4.5 shows the absorption spectra of anthocyanin solution extracted from purple carrot and that of the TiO_2 electrode after being soaked in anthocyanin solution.

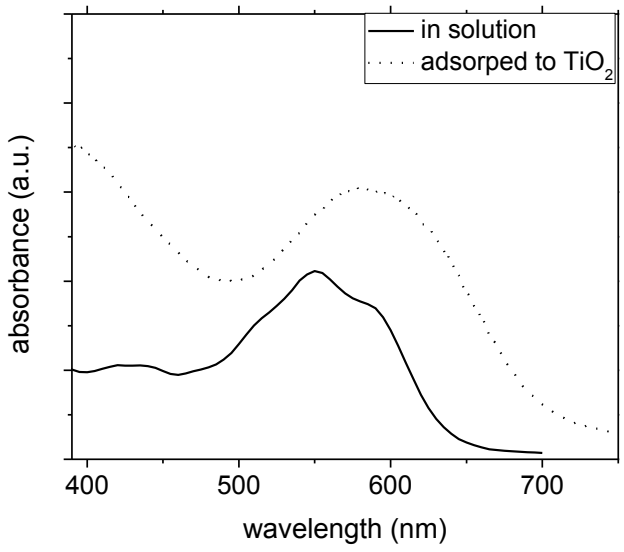

Fig. 4.5 Absorption spectra of purple carrot extract in ethanol solution and anthocyanin adsorbed onto TiO_2 film.

The absorption spectrum for the anthocyanin dye in solution shows a main peak at wavelength of 552 nm. It can be observed that the absorption band of anthocyanin/TiO_2 is red shifted towards higher wavelength (584 nm) compared to that of the anthocyanin in solution. The shift towards lower energy can be attributed to complexation between anthocyanin and metal ions, Ti^{4+} [49].

As shown in Table 4.1 the efficiency of the DSSC sensitized with Ru is 1.35%. Even though the efficiency values obtained in this study are not very close to the values obtained for the DSSC sensitized with the very expensive Ruthenium complexes, the preparation of DSSCs sensitized by natural dyes still allows the possibility of producing cheaper and environmentally friendly solar cells. Therefore, investigations are being carried out in searching for efficient natural dyes which can have potential use in these DSSCs [44].

4.2.2 Optimization of the Extracting Temperature of the Dye from Purple Carrot

4.2.2.1 Experiment

The performance of the DSSC is crucially dependent on many parameters. Among these parameters is the temperature at which the dye is extracted. One gram of purple carrot was immersed in 10 ml of ethanol at five different extracting temperatures which are 25^oC, 40^oC, 50^oC, 60^oC, and 70^oC using an oven as shown in Fig. 4.6 and kept in the dark for one day. Then the fabricated TiO_2 films were soaked in these dyes for one day. After assembling the DSSCs, the photovoltaic parameters were studied.

Fig. 4.6 The purple carrot dye solution at five different extracting temperatures.

4.2.2.2 Results and Discussions

❖ Absorption Spectra of the Extract of Purple Carrot

The UV–Vis absorption spectra of the extract of purple carrot at different temperatures were measured and the results are shown in Fig. 4.7.

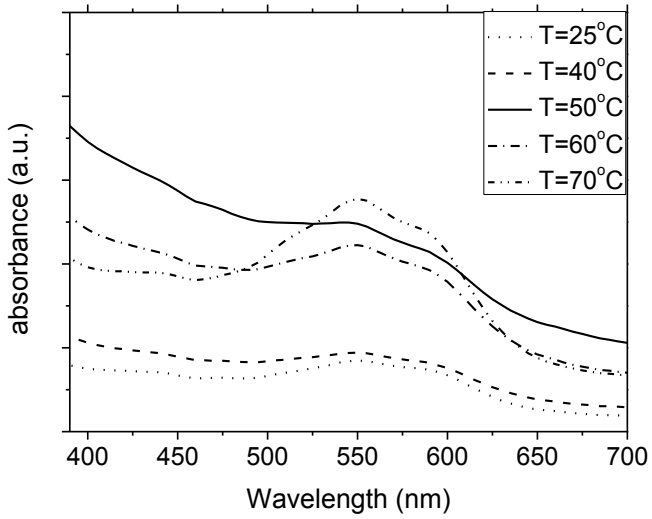

Fig. 4.7 The UV–Vis absorption spectra of the extract of purple carrot at different extracting temperatures.

❖ J-V Characterization of DSSCs Sensitized by Purple Carrot at Different Extracting Temperatures

The photovoltaic parameters of the fabricated DSSCs were tested and listed in Table 4.2. Figures 4.8 and 4.9 show the J-V characteristic curves and the power of DSSCs fabricated with purple carrot at different extracting temperatures.

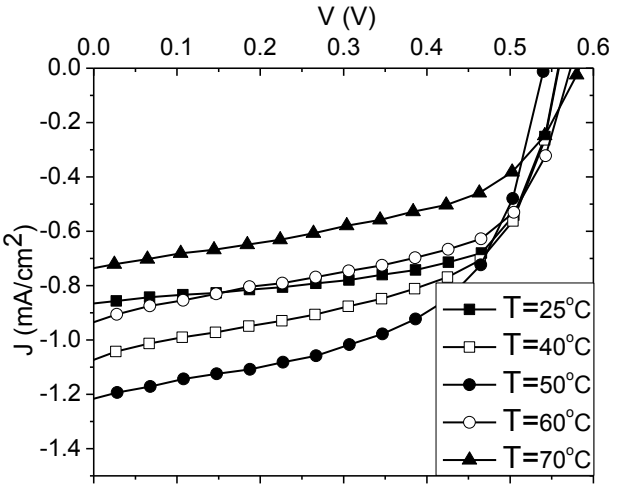

Fig. 4.8 Current density (J) versus voltage (V) characteristics curves for the DSSCs sensitized at different extracting temperatures.

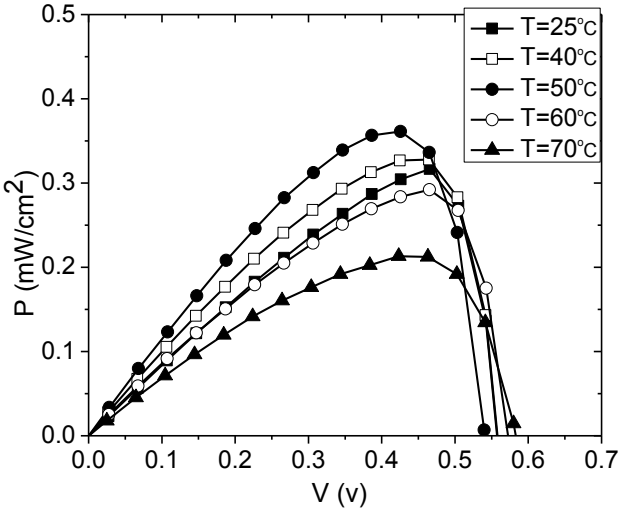

Fig. 4.9 Power (P) versus voltage (V) characteristics curves of the DSSCs sensitized at different extracting temperatures.

Table 4.2 Photovoltaic parameters of the DSSCs sensitized by purple carrot at different extracting temperatures.

Extracting Temperature	J_{sc} (mA/cm^2)	V_{oc} (V)	J_m (mA/cm^2)	V_m (V)	FF	η %
25	0.87	0.56	0.68	0.47	0.65	0.31
40	1.07	0.56	0.74	0.44	0.55	0.33
50	1.21	0.54	0.87	0.42	0.55	0.36
60	0.93	0.57	0.62	0.46	0.54	0.29
70	0.74	0.59	0.49	0.44	0.50	0.22

Figure 4.10 shows the DSSC efficiency as a function of the extracting temperature. As observed from the figure, the efficiency is enhanced with increasing the extracting temperature from 25°C to 50°C and then it declines towards lower values with further increasing of the temperature. An extracting temperature of 50°C could be used as an optimal value and the reason behind that may be attributed to the increase of the optical absorption of the dye in the range 400-550 nm, as shown in Fig. 4.7.

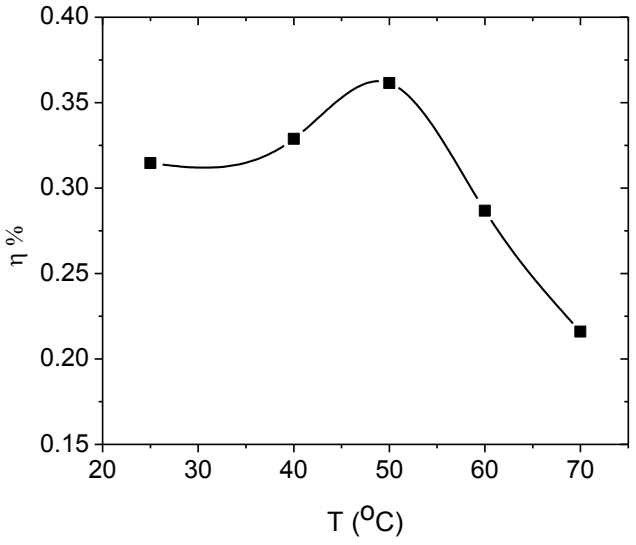

Fig. 4.10 DSSC efficiency (η) versus the extracting temperature (T) of purple carrot extract.

4.2.3 Effect of the pH of the Dye Solution on DSSCs Efficiency

4.2.3.1 Experiment

To investigate the effect of the pH on the performance of purple carrots extracts as photosensitizers, dyes were treated with acetic and hydrochloric acid. The original pH of the purple carrot extracts in Ethanol was around 7.4 using pH meter. Five different pH values ranging from 2.8 to 7.4 were examined by adding acetic acid (0.1 M) to the dye solutions. On the other hand, 0.1 M of hydrochloric acid was added to the dye solutions in order to get six different values of pH ranging from 7.4 to a minimum value of 1 as shown in Fig. 4.11.

Fig. 4.11 The treatment of the purple carrot dye solutions using acetic and hydrochloric acids.

4.2.3.2 Results and Discussions

❖ **Absorption Spectra of Various Extracts at Different pH**

The absorption spectra of purple carrot extracts at different pH values were measured and shown in Fig. 4.12 for acetic acid and Fig. 4.13 for hydrochloric acid. The values of pH of

purple carrot extracts using acetic acid are 7.4, 5.8, 4.8, 3.8, and 2.8 whereas the pH values of the dye extracts using hydrochloric acid are 7.4, 6.4, 5, 3.6, 2.1, and 1.

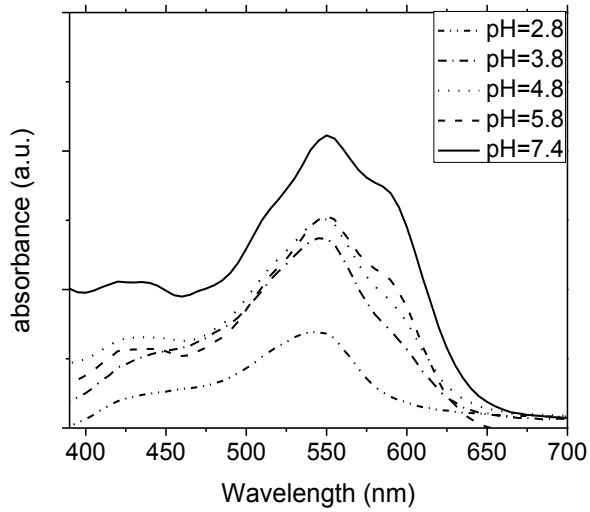

Fig. 4.12 Absorption spectra of purple carrot extract solutions at various pH values using acetic acid.

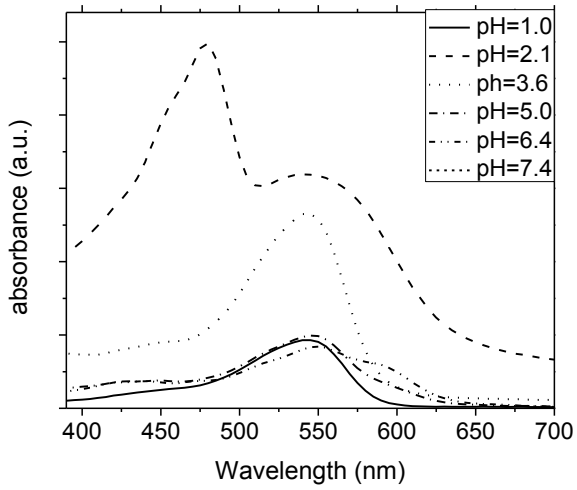

Fig. 4.13 Absorption spectra of purple carrot extract solutions at various pH levels using hydrochloric acid.

❖ J-V Characterization of DSSCs sensitized with Extracts of Purple Carrot at Different Values of pH

The J-V characteristics of DSSCs sensitized with extracts of purple carrot at different

values of pH using acetic and hydrochloric acids are shown in Fig. 4.14 and Fig. 4.15, respectively. Moreover, the power is shown for all DSSCs using the extract of purple carrot at different pH values using acetic and hydrochloric acids in Fig. 4.16 and Fig. 4.17, respectively.

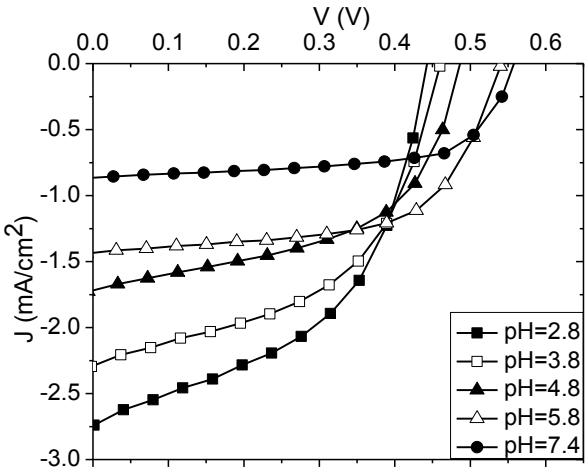

Fig. 4.14 Current density (J) versus voltage (V) characteristic curves for DSSCs sensitized with purple carrot extract solutions at various pH values using acetic acid.

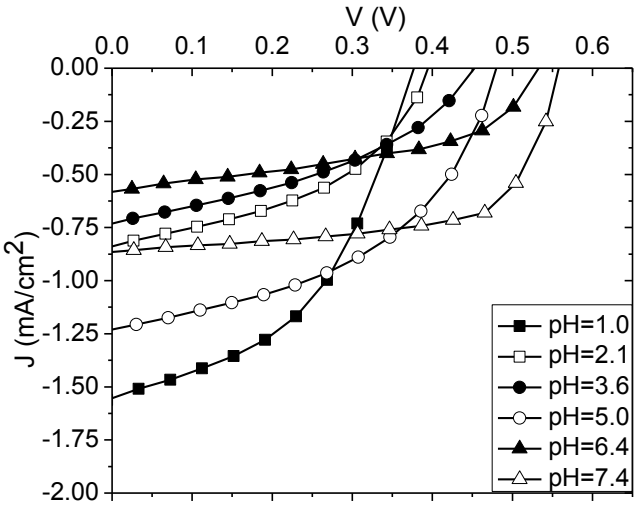

Fig. 4.15 Current density (J) versus voltage (V) characteristic curves for DSSCs sensitized with purple carrot extract solutions at various pH values using hydrochloric acid.

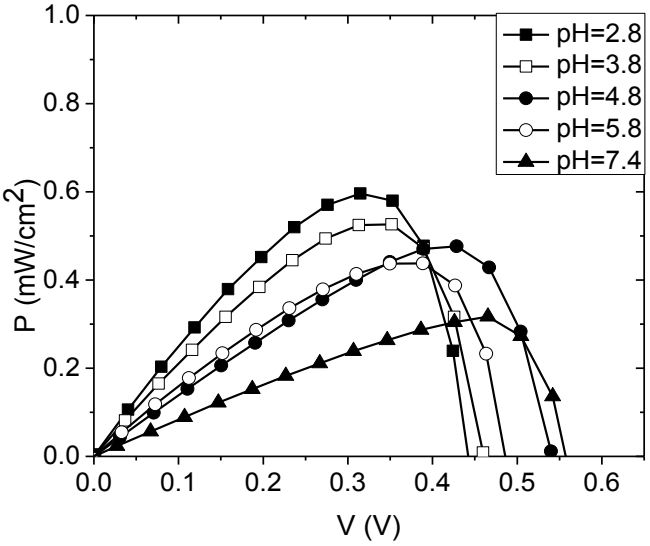

Fig. 4.16 Power (P) versus voltage (V) characteristic curves for DSSC sensitized with purple carrot dye solutions of various pH values using acetic acid.

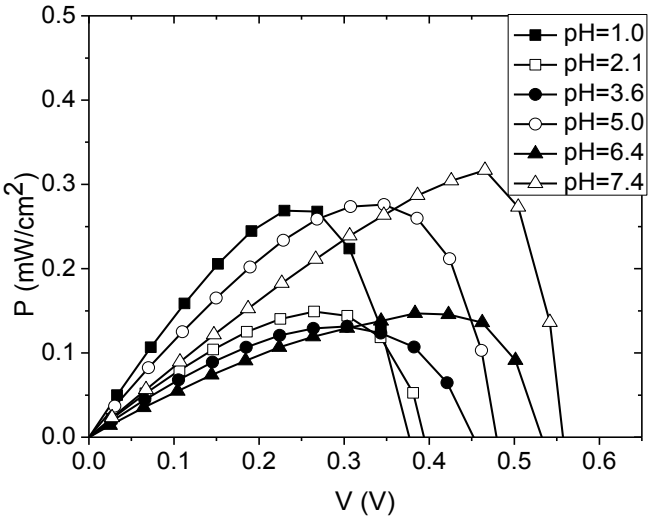

Fig. 4.17 Power (P) versus voltage (V) characteristic curves for DSSC sensitized with purple carrot dye solutions of various pH values using hydrochloric acid.

Figure 4.18 shows the DSSC efficiency as a function of the pH values of the extract solutions of purple carrot using acetic acid. As observed from the figure, the efficiency is enhanced dramatically with decreasing the pH values from 7.4 to the lowest value of 2.8 which corresponds the highest efficiency. Table 4.3 shows the photovoltaic parameters of

the DSSCs sensitized by purple carrot at different pH values using acetic.

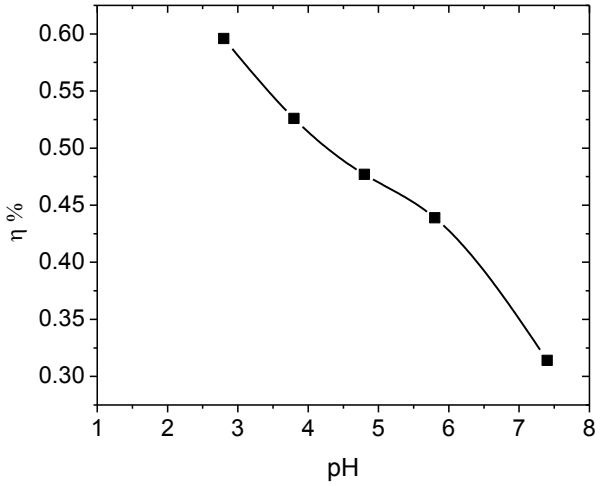

Fig. 4.18 DSSC efficiency versus the pH of the extract solution of purple carrot using acetic acid.

Table 4.3 Photovoltaic parameters of the DSSCs sensitized by purple carrot at different pH vales using acetic acid.

pH (Acetic)	J_{sc} (mA/cm^2)	V_{oc} (V)	J_m (mA/cm^2)	V_m (V)	FF	η %
7.4	0.87	0.56	0.68	0.47	0.65	0.31
5.8	1.72	0.49	1.16	0.38	0.52	0.44
4.8	1.44	0.54	1.12	0.43	0.61	0.48
3.8	2.29	0.46	1.59	0.33	0.50	0.53
2.8	2.75	0.44	1.90	0.31	0.49	0.60

Figure 4.19 shows the DSSC efficiency as a function of the pH of the purple carrot extract solutions using hydrochloric acid. As observed from Fig 4.20, the efficiency is diminished with decreasing the pH from 7.4 to 6.4 then enhanced from 6.4 to 5 pH values, after that it declines towards lowest value at pH=3 then return to increase with further decreasing of the pH to the lowest values. Table 4.4 shows the photovoltaic parameters of the DSSCs

sensitized by purple carrot at different pH values using hydrochloric acids.

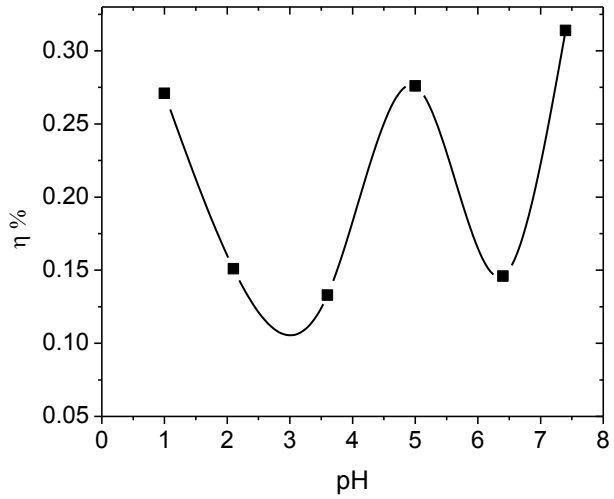

Fig. 4.19 DSSC efficiency versus the pH of the purple carrot extract solution using hydrochloric acid.

Table 4.4 Photovoltaic parameters of the DSSCs sensitized by purple carrot at different pH vales using hydrochloric acid.

pH (Hydrochloric)	J_{sc} (mA/cm^2)	V_{oc} (V)	J_m (mA/cm^2)	V_m (V)	FF	η %
7.4	0.87	0.56	0.68	0.47	0.65	0.31
6.4	0.58	0.38	0.36	0.40	0.67	0.15
5.0	1.23	0.48	0.84	0.33	0.47	0.28
3.6	0.73	0.45	0.44	0.30	0.40	0.13
2.1	0.84	0.40	0.57	0.27	0.46	0.15
1.0	1.55	0.38	1.08	0.25	0.46	0.27

The treatment of the dye solutions with acetic acid resulted in better performance in comparison with the hydrochloric acid treatment because hydrochloric acid is a strong acid compared to acetic acid. In acetic acid treatment in figure 4.12, the absorption intensity

was the same, which confirms that the acid treatment does not affect the absorption of the dye molecules, but it modifies the TiO_2 surface. Our results are in agreement with Jeong et al [50], the acetic acid treated TiO_2 showed more efficiency than the untreated TiO_2 because the acetic acid modified TiO_2 films to have a better morphology than the untreated TiO_2 film, resulting in an increase in cell performance due to the transportation of electrons. At the same time, the hydrochloric acid treated dye adsorbed TiO_2 film shows poor performance in the power conversion efficiency. The hydrochloric acid present in the dye modifies the surface state of the porous film and creates defect centers on the TiO_2 surface. These defects prevent the transfer of electrons to the TiO_2 grid from the excited state of the sensitized dye molecule, which results in lower electron transportation efficiency and a decrease in the photovoltaic performance [51]. Therefore, the efficiency was higher with the acetic acid treated dye than the hydrochloric acid and untreated dye.

4.2.4 Effect of the Pre-Treatment of FTO Glass Substrates on the Efficiency of DSSCs

One of the methods used for improving the performance of DSSCs is the pre-treatment of FTO glass substrates using strong acids. In this section, hydrochloric (HCl), phosphoric (H_3PO_4), or nitric acids (HNO_3) are chosen to be used for cleaning the FTO glass substrates.

4.2.4.1 Experiment

The FTO glass substrates were cleaned by acetone and ethanol, successively for 20 minutes. To investigate the effect of some acids on the DSSCs efficiency, the substrates was immersed in 0.1 M of one of the acids mentioned before at room temperature for 5 min

then washed with ethanol as shown in Fig. 4.20. Following the TiO_2 paste was spread uniformly on the FTO substrates as mentioned before in section 3.2 then, the TiO_2 electrodes were soaked in an ethanol solution of purple carrot dyes at room temperature for 24 hours. Finally, the fabricated DSSCs were connected to the solar cell simulator and I-V measurement systems mentioned in Fig 3.4.

Fig. 4.20 The pre-treatment of the FTO substrates using HCl, H_3PO_4, and HNO_3.

4.2.4.2 Results and Discussions

- **J-V Characterization of DSSCs with the Pre-Treatment of FTO Glass Substrates**

The J–V characteristics of DSSC with the pre-treatment of FTO glass substrate with the three acids under an illumination of 100 mW/cm^2 are shown in Fig. 4.21. The power is plotted versus the voltage for all DSSCs with the pre-treatment of FTO glass substrates with different acids as shown in Fig. 4.22, and Table 4.5 shows the photovoltaic parameters

of the pre-treated DSSCs sensitized by purple carrot with hydrochloric (HCl), phosphoric (H_3PO_4), or nitric acids (HNO_3).

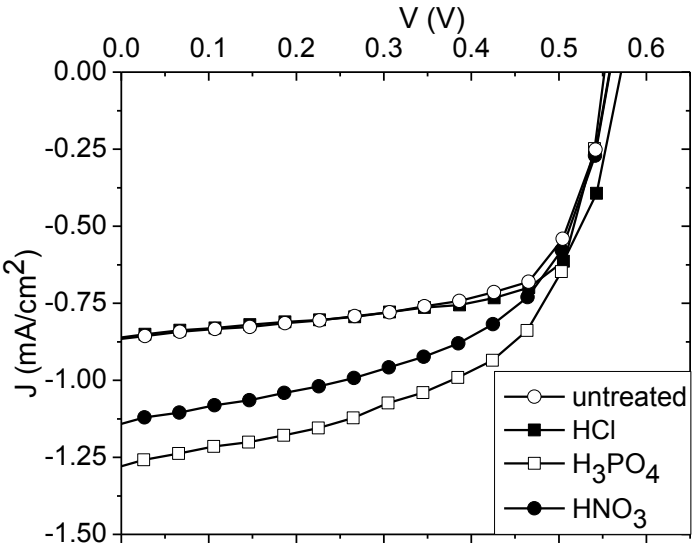

Fig. 4.21 Current density (J) versus voltage (V) characteristic curves of DSSCs with the pre-treatment of FTO glass substrates with HCl, H_3PO_4, and HNO_3 acids.

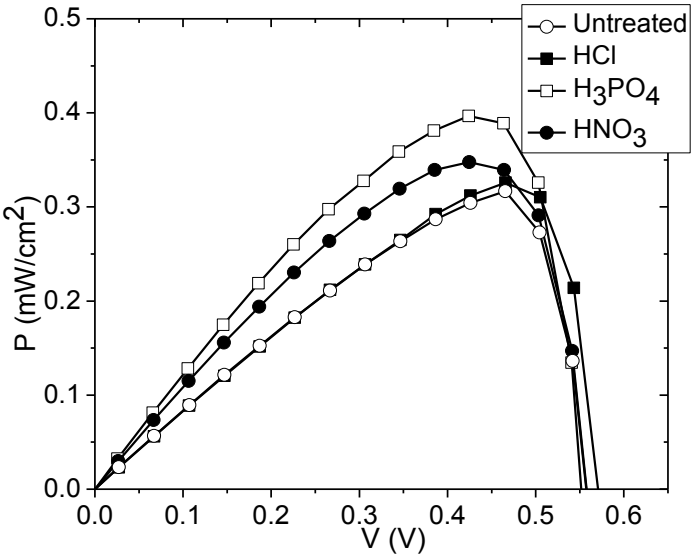

Fig. 4.22 Power (P) versus voltage (V) characteristic curves of the DSSCs with the pre-treatment of FTO glass substrates with HCl, H_3PO_4, and HNO_3 acids.

Table 4.5 Photovoltaic parameters of the DSSCs with the pre-treatment of FTO glass substrates by HCl, H_3PO_4, and HNO_3 acids.

FTO Pre-treatment	J_{sc} (mA/cm^2)	V_{oc} (V)	J_m (mA/cm^2)	V_m (V)	FF	η %
Untreated	0.87	0.56	0.68	0.47	0.65	0.31
HCl (0.1M, 5min)	0.87	0.57	0.70	0.47	0.65	0.32
H_3PO_4 (0.1M, 5min)	1.28	0.55	0.94	0.43	0.57	0.40
HNO_3 (0.1M, 5min)	1.14	0.56	0.82	0.43	0.55	0.35

It is clear that the DSSCs exhibited improved efficiencies after the pre-treatment of the FTO with any of the three acids. The reason behind that may be attributed to the decreasing of the sheet resistance of the FTO glass substrate by acids treatment then the new nanoparticles enhance the surface area and suppress the charge recombination [52]. The pre-treatment of the FTO also increases the contact points between the TiO_2 film and the FTO and improves the electronic interconnection, so that the photoelectrons can be collected efficiently and the probability of electron recombination is reduced. The pre-treatment of the FTO with H_3PO_4 showed an improved efficiency of 130%.

4.2.5 Effect of Surface Post-Treatment of Nanostructured TiO_2 on the Efficiency of DSSCs

Since TiO_2 porous film plays a key role in the enhancement of photoelectric conversion efficiency of DSSCs, many scientists focus their researches on it. Especially, a high light-to-electricity conversion efficiency results from particle size and crystallographic phase,

film porosity, surface structure and surface area to volume ratio of porous TiO_2 electrodes, on which the dye can be sufficiently adsorbed. Effective treatment of the photoelectrode is important to improve DSSCs performance.

4.2.5.1 Experiment

Hydrochloric acid (HCl), phosphoric acid (H_3PO_4), or nitric acid (HNO_3) were used to investigate the effect of surface post-treatment of TiO_2 film on the efficiency of DSSCs. FTO glass plates were cleaned in detergent solution using an ultrasonic bath for 20 min, rinsed with water and acetone and dried in ambient conditions. Nanoporous TiO_2 working electrodes were prepared on FTO substrates form the paste by a doctor blade method. The electrodes were post-annealed at 450^oC for 30 min and cooled down to 100^oC in ambient air. Then, the TiO_2 electrodes were soaked in 0.1 M HCl, H_3PO_4 or HNO_3 at room temperature for 5 min followed by washing with ethanol as shown in Fig. 4.23. After the treatments, the TiO_2 electrodes were soaked in an ethanol solution of purple carrot dyes at room temperature for 24 hours.

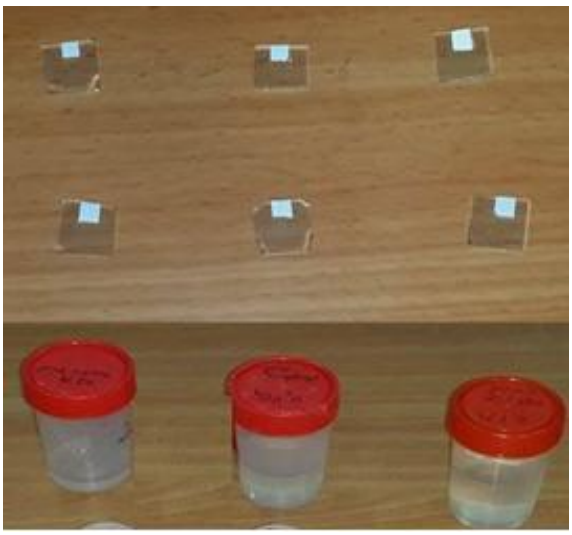

Fig. 4.23 The post-treatment of the TiO_2 film using HCl, H_3PO_4, and HNO_3.

4.2.5.2 Results and Discussions

❖ J-V Characterization of DSSCs with post-treatment of TiO_2 electrode

DSSCs with electrodes that untreated with acids, together with post-treated TiO_2 electrodes are tested under 100 mW/cm^2 intensity. Their characteristic J-V curves are represented in Fig. 4.24 and listed in Table 4.6. The power versus the voltage for all DSSCs with post-treatment of TiO_2 electrode with the three acids are shown in Fig. 4.25.

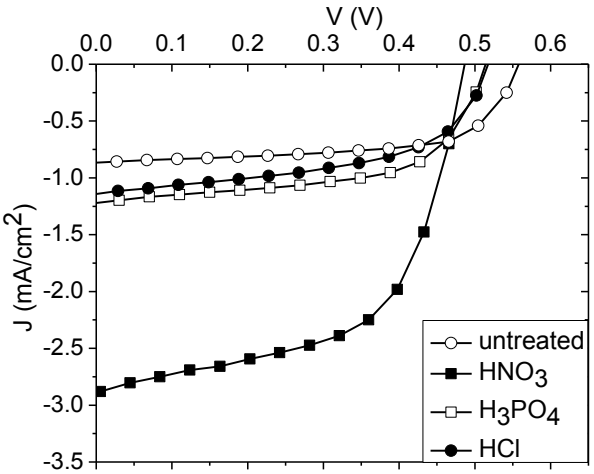

Fig. 4.24 Current density (J) versus voltage (V) characteristic curves of DSSCs with post-treatment of TiO_2 electrode with the three acids.

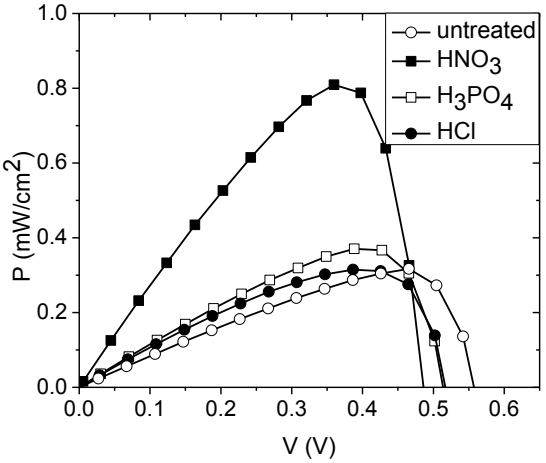

Fig. 4.25 Power (P) versus voltage (V) characteristic curves of the DSSCs with post-treatment of TiO_2 electrode with the three acids.

Table 4.6 Photovoltaic parameters of the DSSCs with post-treatment of TiO_2 electrode by the three acids.

TiO_2 post-treatment	J_{sc} (mA/cm^2)	V_{oc} (V)	J_m (mA/cm^2)	V_m (V)	FF	η %
Untreated	0.87	0.56	0.68	0.47	0.65	0.31
HCl (0.1M, 5min)	1.15	0.52	0.80	0.39	0.54	0.32
H_3PO_4 (0.1M, 5min)	1.22	0.51	0.96	0.39	0.60	0.38
HNO_3 (0.1M, 5min)	2.90	0.49	2.24	0.36	0.57	0.81

Acid post-treated cells exhibited enhanced J_{sc} in comparison with untreated cells. DSSCs treated with HCl, H_3PO_4 or HNO_3 showed J_{sc} values of 1.15, 1.22 and 2.90 mA/cm^2 and reduced V_{oc} values of 0.52 V, 0.51 V and 0.49 V, respectively. HNO_3 treated cells showed the best efficiency of η=0.81%, J_{sc}=2.90 mA/cm^2, V_{oc}=0.49 V and FF=0.57. (The untreated cell gave an efficiency of η=0.31%, J_{sc}=0.87 mA/cm^2, V_{oc}=0.56 V and FF=0.65). The HNO_3 treated cells showed an efficiency enhancement of about 250%.

These observations could be conferring that the acid contributed regular arrangement of the photoelectrode by the dispersion of TiO_2 nanoparticles. This dispersion is one of the factors that makes much chemisorption site for the organic dyes. Also, the reason behind that behavior may be attributed to the improvement of TiO_2 film electrical conductivity by enhancing the neck points between the nanoparticles, increasing dye loading and minimizing the recombination rate between the TiO_2 film and the mediator [53]. The positively charged TiO_2 surface formed by nitric acid treatment induces high electrostatic attraction between the reaction sites and anionic dyes, resulting in a much faster adsorption reaction [54].

4.3 Electrochemical Impedance Spectroscopy (EIS) Analysis

In order to study the internal resistances and electron transfer kinetics of the cells sensitized by purple carrot, EIS was employed for three studies using AUT 85276 Potentiostat-Galvanostat with FRA 32 Module. DSSCs, sensitized by purple carrot without treatment, sensitized by purple carrot of pH 2.8 with acetic acid and sensitized purple carrot dye and FTO treated with nitric acid, were studied.

4.3.1 EIS of the DSSC Sensitized by Purple Carrot without Any Treatment

The EIS measurements were carried out in the dark and under an illumination of 100 mW/cm^2 for the DSSC sensitized by purple carrot without any treatment at -0.4 V, -0.6 V, and -0.8 V applied voltages as shown in Fig. 4.26.

As observed from Fig. 4.26 and Table 4.7, there is a decrease in the charge-transfer resistance (R_{CT}) upon exposure an illumination of 100 mW/cm^2 for the DSSC sensitized by purple carrot without any treatment at the chosen applied voltages. This can be ascribed to a difference in the local I_3^- concentration. Under illumination, I_3^- is formed "in situ" by dye regeneration at the mesoporous TiO_2/electrolyte interface, whereas in the dark, I_3^- is generated at counter electrode and penetrates the mesoporous TiO_2 films by diffusion [55]. Electrochemical circle fit was obtained for the DSSC sensitized by purple carrot without any treatment in the dark and under an illumination at chosen applied voltage as shown in Fig 4.27. Hus and Mansfeld proposed equation 4.1 that can be used to calculate the estimated interfacial capacitance from a depressed semicircle model (a Constant Phase Element in parallel with a resistor) [56].

$$C = Q_0(\omega_{max})^{(n-1)} \quad (4.1)$$

where C is estimated interfacial capacitance, Q_o is the CPE coefficient, ω_{max} is the characteristic frequency at which the imaginary part of the impedance reaches its maximum magnitude, and n is the exponent. A summary of the equivalent circuit component values obtained from modeling the DSSCs sensitized by purple carrot without any treatment in the dark and under an illumination at chosen applied voltage can be found in Table 4.7.

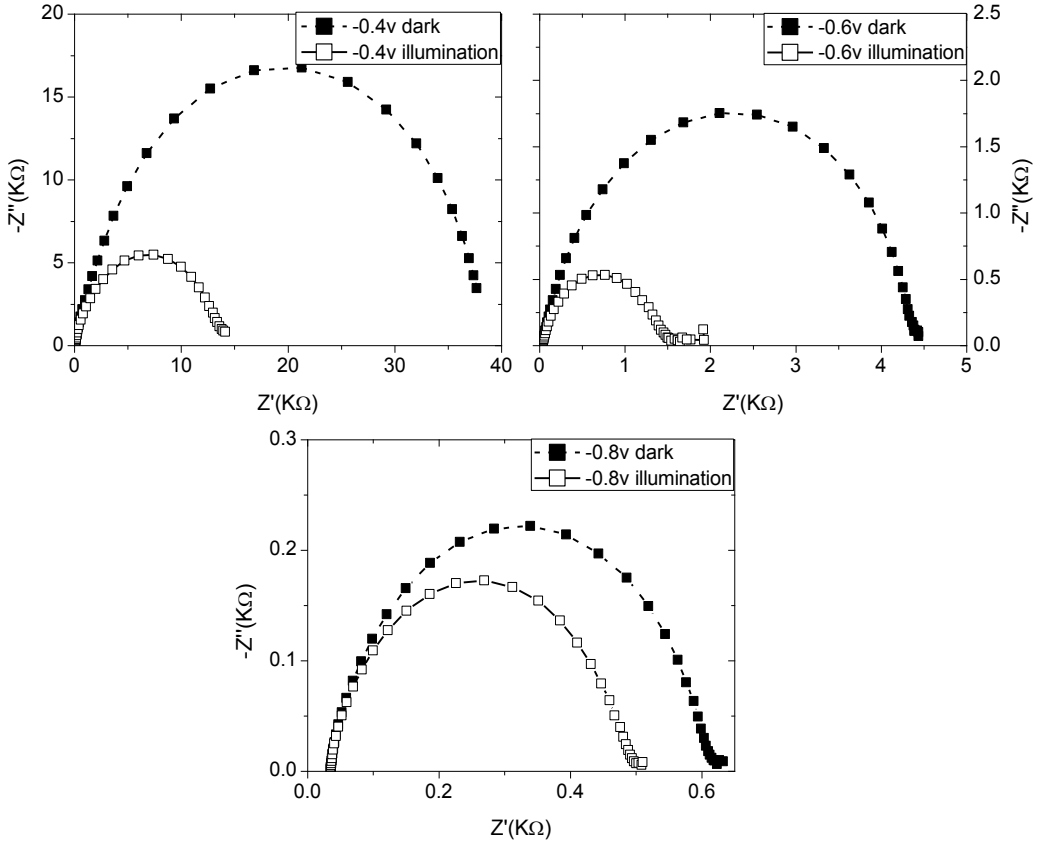

Fig. 4.26 Nyquist plots of the DSSC sensitized by purple carrot without any treatment at -0.4 V, -0.6 V, and -0.8 V in the dark and under an illumination of 100 mW/cm^2.

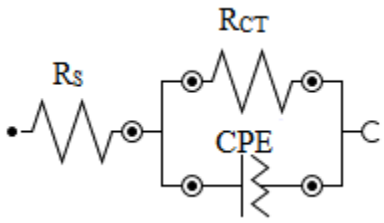

Fig. 4.27 The equivalent circuit for the DSSCs sensitized by purple carrot without any treatment.

Where R_S is the series resistance, CPE is the constant phase element, and R_{CT} is the charge-transfer resistance.

Table 4.7 EIS results from data-fitting of Nyquist plots to the equivalent circuit model in Fig. 4.26

Without treatment	$R_S(\Omega)$	R_{CT} (kΩ)	C(µF)
-0.4v dark	34.70	40.90	3.16
-0.4v illumination	34.20	13.90	2.79
-0.6v dark	34.60	4.42	1.85
-0.6v illumination	33.30	1.52	1.77
-0.8v dark	34.20	0.59	1.28
-0.8v illumination	33.70	0.48	1.29

4.3.2 EIS for DSSC Sensitized by Purple Carrot of pH 2.8 with Acetic Acid

Figure 4.28 shows the Nyquist plots for DSSC sensitized by purple carrot of pH 2.8 with acetic acid in the dark and under an illumination of 100 mW/cm^2 at -0.4 V, -0.6 V, and -0.8 V applied voltages. Electrochemical circle fit were obtained for the DSSCs sensitized by purple carrot of pH 2.8 with acetic acid in the dark at -0.4 V, -0.6 V, and -0.8 V applied

voltages as shown in Fig 4.29. A summary of the equivalent circuit component values obtained from modeling the DSSCs sensitized by purple carrot of pH 2.8 with acetic acid in the dark and under an illumination at chosen applied voltage can be found in Table 4.8. According to Fig 4.29 and Table 4.8, there is an increase in the charge-transfer resistance (R_{CT}) upon exposure an illumination of 100 mW/cm^2 of the DSSC sensitized by Purple carrot of pH 2.8 with acetic acid at -0.4 V applied voltage, whereas at -0.6 V and -0.8 V slightly no different in the R_{CT} upon exposure an illumination of 100mW/cm^2 of the DSSC sensitized by purple carrot of pH 2.8 with acetic acid.

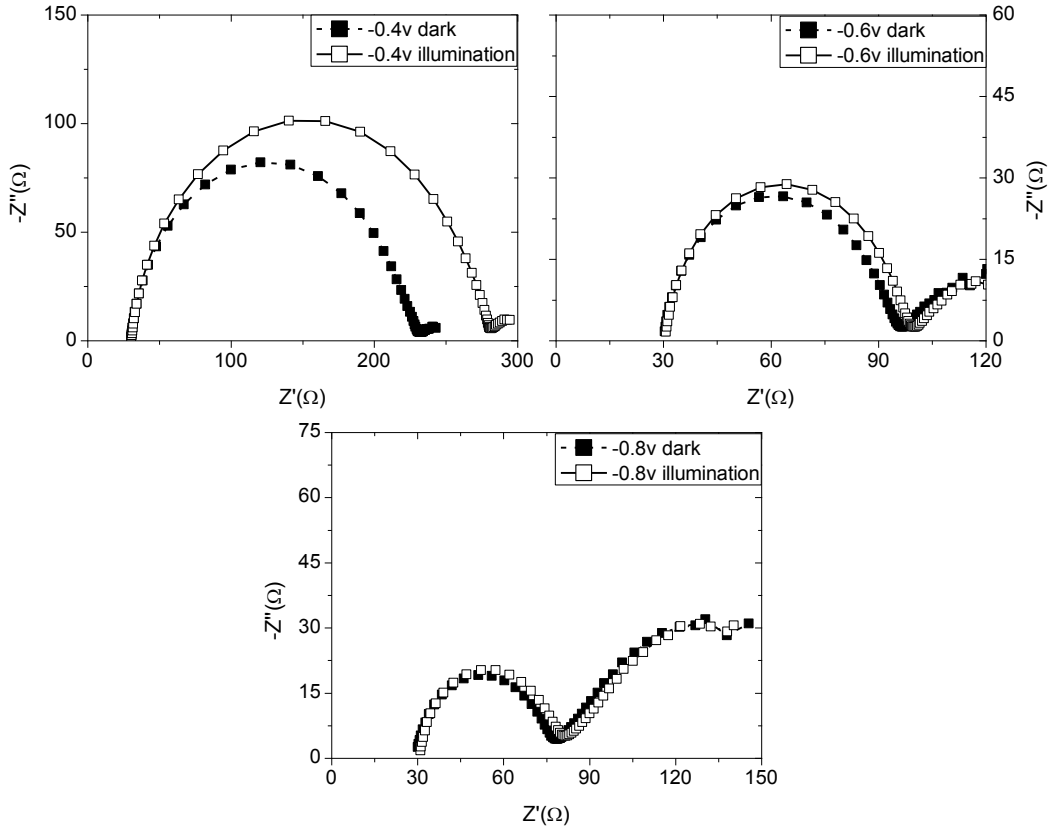

Fig. 4.28 Nyquist plots of the DSSC sensitized by purple carrot of pH 2.8 with acetic acid at -0.4 V, -0.6 V, and -0.8 V in the dark and under an illumination of 100 mW/cm^2.

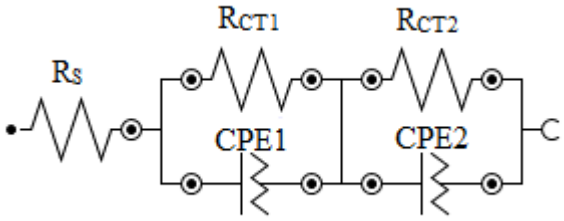

Fig. 4.29 The equivalent circuit for the DSSC sensitized by purple carrot of pH 2.8 with acetic acid.

Table 4.8 EIS results from data-fitting of Nyquist plots to the equivalent circuit model in Fig. 4.28 for the DSSC sensitized by purple carrot of pH 2.8 with acetic acid.

pH 2.8 with acetic acid	$R_S(\Omega)$	$R_{CT1}(\Omega)$	$C_1(\mu F)$	$R_{CT2}(\Omega)$	$C_2(\mu F)$
-0.4v dark	30.1	28.10	149.87	191	2.50
-0.4v illumination	30.1	245	1.18	50.9	45625.82
-0.6v dark	31.7	62.7	0.93	24.3	11900
-0.6v illumination	31.9	66.1	0.92	23.7	14300
-0.8v dark	29.4	46.9	0.86	141	8966.09
-0.8v illumination	30.5	47.1	0.87	183	13585.55

4.3.3 EIS for DSSC Sensitized with Purple Carrot and FTO Pre-Treatment with Nitric Acid (HNO_3).

Figure 4.30 shows the Nyquist plots for DSSC sensitized by purple carrot and pre-treatment of FTO glass substrates with nitric acid in the dark at -0.4 V, -0.6 V, and -0.8 V applied voltages. Electrochemical circle fit was obtained for the DSSCs sensitized by purple carrot

and pre-treatment of FTO glass substrates with nitric acid in the dark at different applied voltages as shown in Fig 4.27. A summary of the equivalent circuit component values obtained from modeling the DSSCs sensitized by purple carrot and pre-treatment of FTO glass substrates with nitric acid in the dark and under an illumination at chosen applied voltage can be found in Table 4.9.

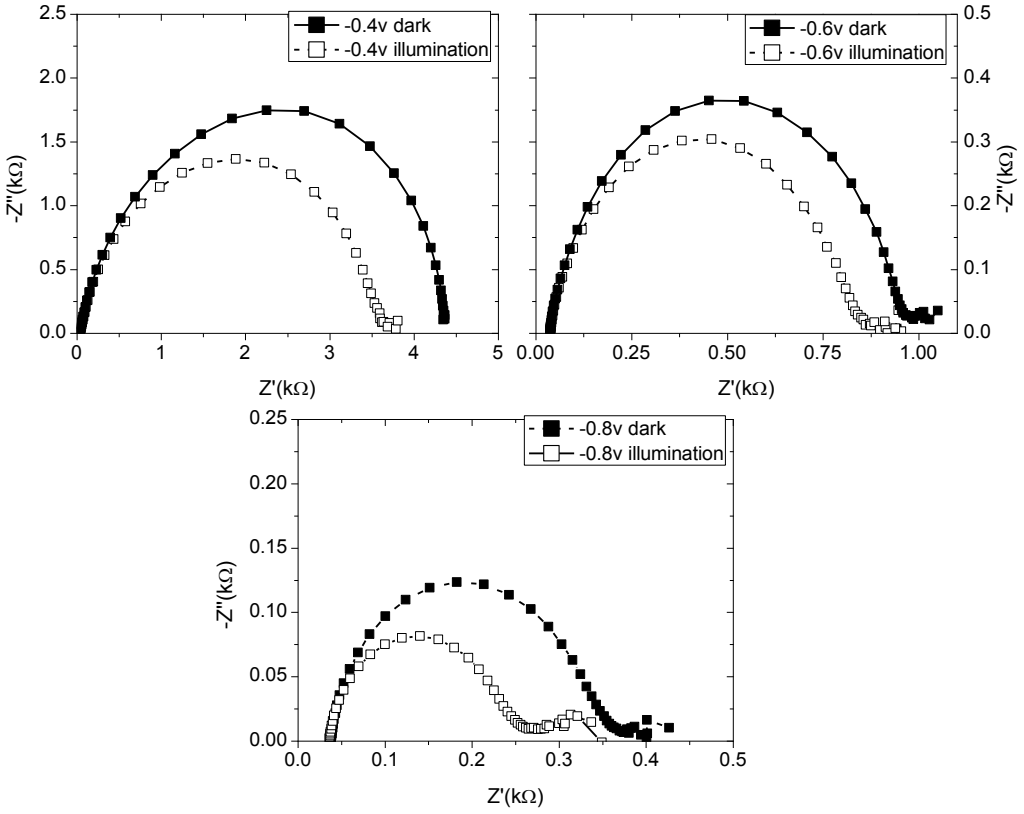

Fig. 4.30 Nyquist plots of the DSSC sensitized by purple carrot with nitric acid pre-treatment of FTO glass substrates at -0.4 V, -0.6 V, and -0.8 V.

Table 4.9 EIS results from data-fitting of Nyquist plots to the equivalent circuit model in Fig. 4.30 for the DSSC sensitized by purple carrot with nitric acid pre-treatment of FTO glass substrates.

Pre-treatment of FTO with HNO_3	$R_S(\Omega)$	$R_{CT}(k\Omega)$	$C(\mu F)$
-0.4v dark	37.0	3.63	2.00
-0.4v illumination	36.1	4.43	2.18
-0.6v dark	36.9	0.83	1.26
-0.6v illumination	36.1	0.94	1.29
-0.8v dark	37.0	0.33	0.94
-0.8v illumination	34.4	0.24	1.02

4.3.4 EIS for DSSCs Sensitized with Purple Carrot for The Three Studies under an Illumination of 100 mW/cm^2 at Same Applied Voltage

Based on Figures. 4.31, 4.32, and 4.33 which represent Nyquist plots of DSSCs sensitized by purple carrot for the three studies mentioned under an illumination of 100 mW/cm^2 at - 0.4 V, -0.6 V, and -0.8 V applied voltages. The inset figures represent Nyquist plots of DSSCs sensitized by purple carrot at pH of 2.8 using acetic acid. EIS is a useful method for the analysis of charge-transport processes and internal resistances [57]. As shown in these Figures, there is a decrease in the R_{CT} for DSSC sensitized by purple carrot of pH 2.8 with acetic acid and pre-treatment of FTO glass substrates with nitric acid compared with the DSSC without any treatment. This increases the number of injected electrons into the TiO_2 film, improves the electrical conductivity, and reduces the charge recombination at the TiO_2/dye/electrolyte interface [58,59].

Giving the data in Fig. 4.34, which represents Bode plots for the DSSCs sensitized by purple carrot for the three studies under an illumination of 100 mW/cm^2 at -0.4 V, -0.6 V, and -0.8 V applied voltages, the reduction of R_{CT} means there is a decrease in the recombination rate and indicates fast electron-transfer processes in the DSSCs sensitized by purple carrot of pH 2.8 with acetic acid and pre-treatment of FTO glass substrates with nitric acid compared with the DSSC without any treatment as indicated in Table 4.13 and that explains the improvement of the efficiency. The efficient charge-transfer paths decrease the recombination rate of electrons with I_3^- or the oxidizing dye, resulting in a high photocurrent density and conversion efficiency [60].

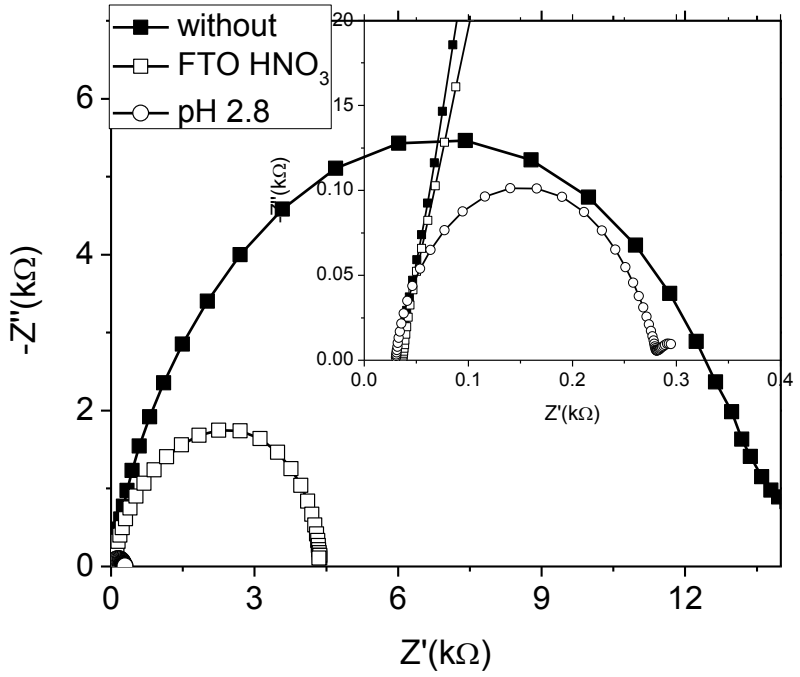

Fig. 4.31 EIS Nyquist plots of DSSC sensitized by purple carrot without any treatment (without), DSSC sensitized by purple carrot at pH of 2.8 using acetic acid (pH 2.8), and DSSC sensitized by purple carrot with pre-treatment of FTO using nitric acid (FTO HNO3) at -0.4 V applied potential under bias illumination of 100 mW/cm^2.

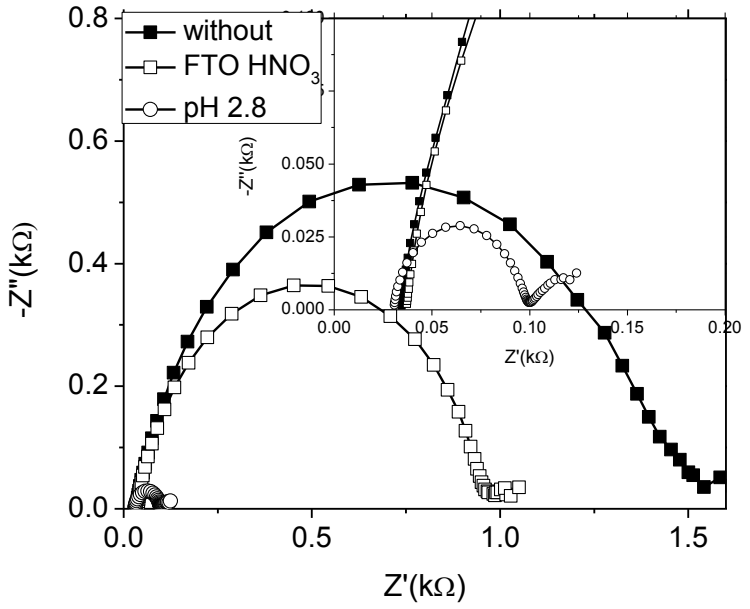

Fig. 4.32 EIS Nyquist plots of DSSC sensitized by purple carrot without any treatment (without), DSSC sensitized by purple carrot at pH of 2.8 using acetic acid (pH 2.8), and DSSC sensitized by purple carrot with pre-treatment of FTO using nitric acid (FTO HNO_3) at -0.6 V applied potential under bias illumination of 100 mW/cm^2.

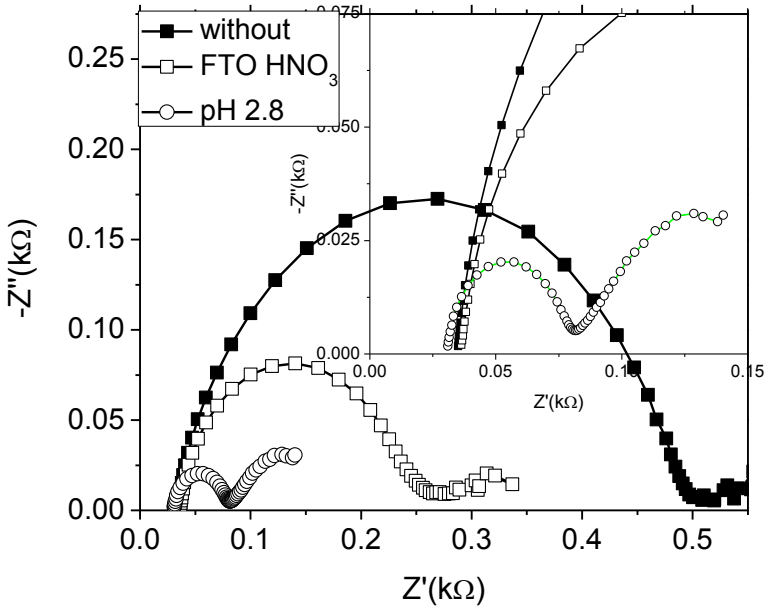

Fig. 4.33 EIS Nyquist plots of DSSC sensitized by purple carrot without any treatment (without), DSSC sensitized by purple carrot at pH of 2.8 using acetic acid (pH 2.8), and DSSC sensitized by purple carrot with pre-treatment of FTO using nitric acid (FTO HNO_3) at -0.8 V applied potential under bias illumination of 100 mW/cm^2.

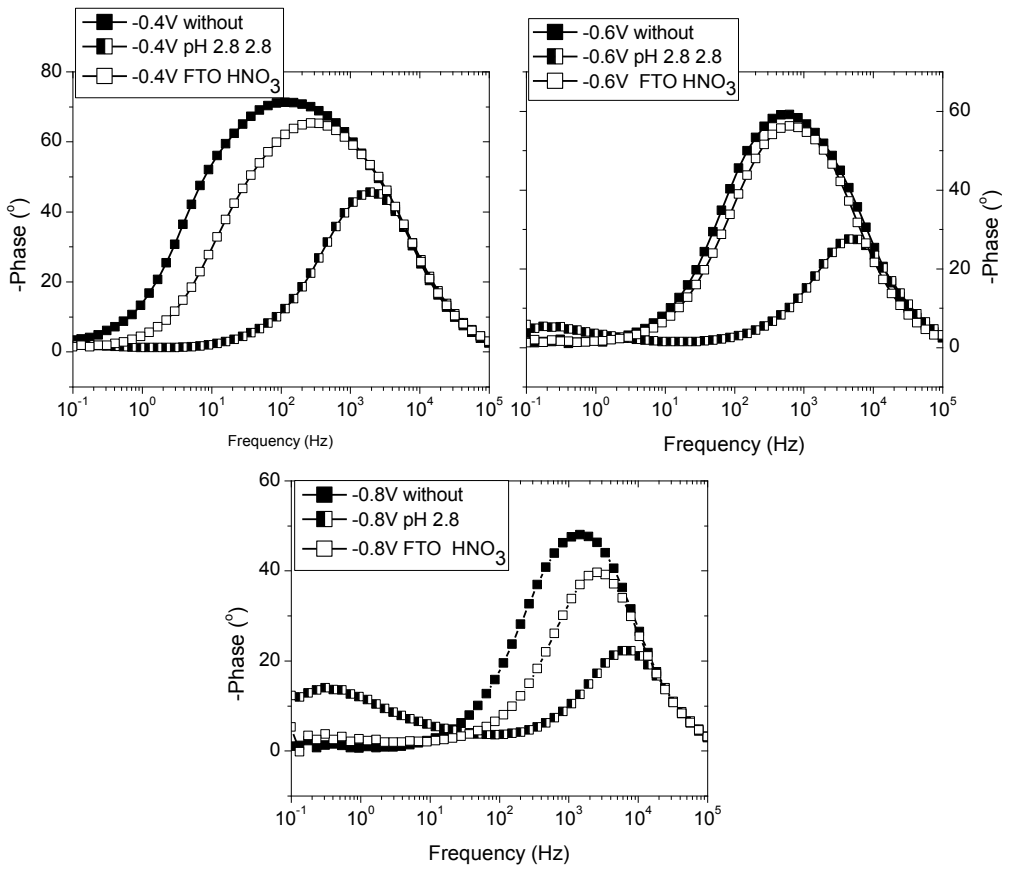

Fig. 4.34 Bode plots of DSSCs sensitized by purple carrot for the three studies mentioned before under an illumination of 100 mW/cm^2 at -0.4 V, -0.6 V, and -0.8 V applied voltages.

Table 4.10 EIS results from data-fitting of Nyquist plots to the equivalent circuit model in Fig. 4.31 for the DSSCs sensitized by purple carrot at -0.4 V applied voltage.

The treatment at -0.4V illumination	$R_S(\Omega)$	R_{CT} (kΩ)	C(μF)	R_{CT2}(kΩ)	C_2(μF)
without treatment	34.20	13.90	2.79		
nitric acid pre-treatment of FTO	36.1	4.43	2.18		
pH 2.8 with acetic acid	30.1	0.25	1.18	0.05	45625.82

Table 4.11 EIS results from data-fitting of Nyquist plots to the equivalent circuit model in Fig. 4.32 for the DSSCs sensitized by purple carrot at -0.6 V applied voltage.

The treatment at -0.6V illumination	$R_S(\Omega)$	R_{CT} (kΩ)	C(µF)	R_{CT2}(kΩ)	C_2(µF)
without treatment	33.30	1.52	1.77		
nitric acid pre-treatment of FTO	36.1	0.94	1.29		
pH 2.8 with acetic acid	31.9	0.07	0.92	0.02	14300

Table 4.12 EIS results from data-fitting of Nyquist plots to the equivalent circuit model in Fig. 4.33 for the DSSCs sensitized by purple carrot at -0.8 V applied voltage.

The treatment at -0.8V illumination	$R_S(\Omega)$	R_{CT} (kΩ)	C(µF)	R_{CT2}(kΩ)	C_2(µF)
without treatment	33.70	0.48	1.29		
nitric acid pre-treatment of FTO	34.4	0.24	1.02		
pH 2.8 with acetic acid	30.5	0.05	0.87	0.18	13585.55

Table 4.13 Electron lifetime calculations from Bode plots.

The treatment	**f (frequency corresponding to peak in Bode plot) (Hz)**	**$\tau_{electron}$ (ms)**
-0.4 V without	115.40	1.38
-0.4 V pH 2.8	1930.70	0.08
-0.4 V FTO HNO_3	268.27	0.59
-0.6 V without	625.06	0.25
-0.6 V pH 2.8	4498.40	0.04
-0.6 V FTO HNO_3	625.06	0.25
-0.8 V without	1456.30	0.11
-0.8 V pH 2.8	5963.60	0.03
-0.8 V FTO HNO_3	2559.50	0.06

CHAPTER FIVE

CONCLUSION

The work in this thesis sought to better understand and establish the necessary steps needed to make solar energy as economically viable as fossil fuels. This thesis concentrates on DSSCs which still relatively new type of photovoltaic cells. DSSCs have the potential to be cheaper than other solar cells and just as efficient.

Six natural dyes extracted from plant roots have been tested as sensitizers for DSSCs. The DSSCs based on purple carrot roots as sensitizers have showed the highest efficiency.

The main aims of this thesis were to study the effect of several parameters on the performance of DSSCs including the optimum extracting temperature of the purple carrot solution which found to be 50°C, also to study the effect of changing the pH values of the dye solution using acetic and hydrochloric acids, and finally to study the influence of pre and post-treatments of the FTO glass substrate and the TiO_2 film using hydrochloric (HCl), phosphoric (H_3PO_4), and nitric (HNO_3) acids.

Better performance was obtained with the acetic acid treatment of the dye solutions than the hydrochloric acid. As observed from the results, the efficiency is enhanced dramatically with decreasing the pH values from 7.4 to the lowest value of 2.8 which corresponds the highest efficiency using acetic acid. The pre-treatment of the FTO with phosphoric acid (H_3PO_4) resulted in improved efficiencies of 130% for the DSSCs sensitized by purple carrot. The nitric acid (HNO_3) post-treated electrodes showed an efficiency of η=0.808%, a short circuit current of J_{sc}=2.903 mA/cm^2, an open circuit voltage of V_{oc}=0.486 V and a fill factor of FF=0.573. (The cell built with untreated electrodes gave an efficiency of η=0.314%, a

short circuit current of J_{sc}=0.866 mA/cm^2, an open circuit voltage of V_{oc}=0.555 V and a fill factor of FF=0.654). The HNO_3 treated electrodes showed an efficiency enhancement of about 250%. These observations could be conferring to that the acid treatment contributed regular arrangement of the photoelectrode by the dispersion of TiO_2 nanoparticles which provides much chemisorption site for the organic dyes. The improvement of TiO_2 film electrical conductivity is achieved by enhancing the neck points between the nanoparticles, increasing dye loading and minimizing the recombination rate between the TiO_2 film and the mediator.

These results clearly show that the application of natural dye to DSSCs as a photosensitizer is promising for the realization of high cell performance, low-cost production, and non-toxicity. It should be emphasized here that natural dyes from food are better for human health than synthetic dyes.

References

[1] M. Gratzel, "Recent Advances in Sensitized Mesoscopic Solar Cells", Accounts of Chemical Research. Vol. 42, No. 11, pp. 1788-1798 (2009).

[2] N. Lewis and D. Nocera, "Powering the planet: Chemical challenges in solar energy utilization", The National Academy of Sciences of the USA, Vol. 103, No. 43, pp. 15729–15735 (2006).

[3] N. Lewis, "Toward cost-effective solar energy use", Science. Vol. 315, No. 5813, pp. 798-801 (2007).

[4] D. Chapin, C. Fuller, and G. Pearson, "A new silicon p-n junction photocell for converting solar radiation into electrical power", Journal of Applied Physics, Vol. 25, No. 5, pp. 676-677 (1954).

[5] Sunlight [online]. http://en.wikipedia.org/wiki/Sunlight

[6] C. Gueymard, D. Myers, and K. Emeryand, "Proposed reference irradiance spectra for solar energy systems testing", Solar Energy, Vol. 73, No. 6, pp. 443-467 (2002).

[7] E. Becquerel, "Memoire sur led effets electriques produits sous I'influence des rayons solaires", Comptes Rendus, Vol. 9 No. 7, pp. 561-567 (1839).

[8] A. Wang, J. Zhao, and M. Green, "24% efficient silicon solar cells", Applied Physics Letters, Vol. 57, No. 6, pp. 605-607 (1990).

[9] M. Green1, K. Emery, Y. Hishikawa, W. Warta, and E. Dunlop, "Solar cell efficiency tables version 39", Progress in Photovoltaics: Research and Applications, Vol. 20, No. 1, pp. 12-20 (2011).

[10] J. Britt and C. Ferekides, "Thin film CdS/CdTe solar cell with 15.8% efficiency", Applied Physics Letters, Vol. 62, No. 22, pp. 2851-2853 (1993).

[11] M. Green, K. Emery, Y. Hishikaw,a and W. Warta, "Solar cell efficiency tables version 37", Progress in Photovoltaics: Research and Applications, Vol. 19, No. 1, pp. 84-92 (2011).

[12] H. Cotal, C. Fetzer, J. Boisvert, G. Kinsey, R. King, P. Hebert, H. Yoon, and N. Karam, "III–V multijunction solar cells for concentrating photovoltaics", Energy & Environmental Science, Vol. 2, No. 2, pp. 174–192 (2009).

[13] H. Upadhyaya, S. Senthilarasu, M. Hsu, and D. Kumar, " Recent progress and the status of dye-sensitized solar cell (DSSC) technology with state of the art conversion efficiencies", Solar Energy Materials and Solar Cells, Vol. 119, pp. 291–295 (2013).

[14] S. Forrest, "The Limits to Organic Photovoltaic Cell Efficiency", Materials Research Society, Vol. 30, No. 1, pp. 28-32 (2005).

[15] K. Kalyanasundaram, "Dye-Sensitized Solar Cells", EPFL Press, Lausanne (2010).

[16] M. Green, "Third Generation Photovoltaics: Advanced Solar Electricity Generation", Springer-Verlag, Berlin Heidelberg, (2003).

[17] H. Gerischer, M. E. Michael-Beyerle, F. Rebentrost, and H. Tributsch,"Sensitization of charge injection into semiconductors with large band gap", Electrochimica Acta, Vol. 13, No. 6, pp. 1509-1515 (1968).

[18] H. Tsubomura, M. Matsumura, Y. Nomura, and T. Amamiya, "Dye sensitised zinc oxide: aqueous electrolyte: platinum photocell", Nature, Vol. 261, No. 5559, pp. 402-403 (1976).

[19] K. kalyanasundaram, N. Vlachopoulos, V. Monnier, and M. Gratzel, "Sensitization of titanium dioxide in the visible light region using zinc porphyrins", Physical chemistry, Vol. 91, No. 9, pp. 2342-2347, (1987).

[20] B. O'Regan and M. Gratzel, "A low-cost, high-efficiency solar cell based on dye-sensitized colloidal TiO_2 films", Nature, Vol. 353, No. 24, pp. 737–740 (1991).

[21] N. Cherepy , G. Smestad , M. Gratzel, and J. Zhang, "Ultrafast Electron Injection: Implications for a Photoelectrochemical Cell Utilizing an Anthocyanin Dye-Sensitized TiO_2 Nanocrystalline Electrode", The Journal of Physical Chemistry B, Vol. 101, No. 45, pp. 9342-9351 (1997).

[22] G. Calogero, G. Di Marco, S. Cazzanti, S. Caramori, R. Argazzi, A. Di Carlo, and C. Bignozzi, "Efficient Dye-Sensitized Solar Cells Using Red Turnip and Purple Wild Sicilian Prickly Pear Fruits", International Journal of Molecular Sciences, Vol. 11, No. 1, pp.254-267 (2010).

[23] J. Burschka, N. Pellet, Soo-J. Moon, R. Humphry-Baker, P. Gao, M. Nazeeruddin, and M. Gratzel, "Sequential deposition as a route to high-performance perovskite-sensitized solar cells", Nature, Vol. 499, No. 7458, pp. 316-319 (2013).

[24] H. Kim, Y. Bin, S. Karthick, K. Hemalatha, C. Raj, S. Venkatesan, S. Park, and G. Vijayakumar, "Natural Dye Extracted from Rhododendron Species Flowers as a Photosensitizer in Dye Sensitized Solar Cell", International Journal of Electrochemical Science, Vol. 8, No. 5, pp. 6734-6743 (2013).

[25] A. Abu Jasser, "A Stand-Alone Photovoltaic System, Case Study: A Residence in Gaza", Journal of Applied Sciences in Environmental Sanitation, Vol. 5, No. 1, pp. 81-91 (2010).

[26] M. Gratzel, L. Kavan, J. Moser, and J. Augustynski, "Highly efficient sensitization of titanium-dioxide", American chemistry society, Vol. 107, No. 10, pp. 2988-2990 (1985).

[27] C. Noumissing Sao, "Dye Sensitized Solar Cells Based On Perylene Derivatives", PhD Thesis, University of Kassel (Germany), 2009.

[28] F. Gao, Y. Wang, D. Shi, J. Zhang, M. Wang, X. Jing, R. Humphry-Baker, P. Wang, S. M. Zakeeruddin and M. Grätzel, "Enhance the Optical Absorptivity of Nanocrystalline TiO_2 Film with High Molar Extinction Coefficient Ruthenium Sensitizers for High Performance Dye-Sensitized Solar Cells", American chemistry society, Vol. 132, No. 32, pp. 10720–10728 (2008).

[29] J. Wu, Z. Lan, S. Hao, P. Li, J. Lin, M. Huang, L. Fang, and Y. Huang, "Progress on the electrolytes for dye-sensitized solar cells", Pure and Applied Chemistry, Vol. 80, No. 11, pp. 2241-2258 (2008).

[30] M. Toivola, F. Ahlskog, and P. Lund, "Industrial sheet metals for nanocrystalline dye-sensitized solar cell structures", Solar Energy Materials & Solar Cells, Vol. 90, No. 17, pp. 2881–2893 (2006).

[31] A. Kay, and M. Gratzel, "Low cost photovoltaic modules based on dye sensitized nanocrystalline titanium dioxide and carbon powder", Solar Energy Materials & Solar Cells, Vol. 44, No. 1, pp. 99–117 (1996).

[32] http://honorsfellows.blogs.wm.edu/2013/06/20/solar-cell-efficiency-an-introduction/

[33] J. Asbury, R. Ellingson, H. Ghosh, S. Ferrere, A. Nozik, and T. Lian, "Femtosecond IR study of excited-state relaxation and electron-injection dynamics of Ru $(dcbpy)_2$ $(NCS)_2$ in solution and on nanocrystalline TiO_2 and Al_2O_3 thin films", The Journal of Physical Chemistry B, Vol. 103, No. 16, pp.3110-3119 (1999).

[34] M. Gratzel, "Solar Energy Conversion by Dye-Sensitized Photovoltaic Cells", Inorganic Chemistry, Vol. 44, No. 20, pp. 6841-6851 (2005).

[35] Y. Saito, T. Kitamura, Y. Wada, and S. Yanagida, "Application of Poly (3, 4-ethylenedioxythiophene) to Counter Electrode in Dye-Sensitized Solar Cells", Chemistry Letters, Vol. 31, No. 10, pp. 1060-1061 (2002).

[36] Y. Saito, W. Kubo, T. Kitamura, Y. Wada, and S. Yanagida, "I^-/I_3^- redox reaction behavior on poly(3,4-ethylenedioxythiophene) counter electrode in dye-sensitized solar cells", Journal of Photochemistry and Photobiology A: Chemistry, Vol. 164, No. 1-3, pp. 153-157 (2004).

[37] Basics of Electrochemical Impedance Spectroscopy. Application Note. Gamry Instruments. http://www.gamry.com.

[38] A. Mcevoy, T. Markvart, and L. Castaner, "Practical handbook of photovoltaics: fundamentals and applications", Elsevier Ltd., 2nd ed., 2012.

[39] Ultraviolet–visible spectroscopy
http://en.wikipedia.org/wiki/Ultraviolet%E2%80%93visible_spectroscopy

[40] F. Rouessac and A. Rouessac, "Chemical analysis: modern instrumentation methods and techniques", John Wiley & Sons (Chichester, 2004)

[41] J.R. Meyer-Arendt, "Introduction to Classical and Modern Optics", 4th Ed., Prentice Hall (Englewood Cliffs, 1995).

[42] K. Hara, T. Horiguchi, T. Kinoshita, K. Sayama, H. Sugihara, and H. Arakawa, "Highly efficient photon-to-electron conversion with mercurochrome-sensitized nanoporous oxide a semiconductor solar cells", Solar Energy Materials & Solar Cells, Vol. 64, No. 2, pp. 115-134 (2000).

[43] A. Tolvanen, "Characterization and manufacturing techniques of dye sensitized solar cell", Master of science in technology, HELSINKI UNIVERSITY OF TECHNOLOGY, (FINLAND), (2003).

[44] S. Hao, J. Wu, Y. Huang, and J. Lin, "Natural dyes as photosensitizers for dye-sensitized solar cell", Solar Energy, Vol. 80, No. 2, pp. 209–216 (2006).

[45] B. A. Cevallos-Casals, and L. Cisneros-Zeballos, "Stability of Anthocyanin Based Aqueous Extract of Andean Purple Corn and Red Fleshed Sweet Potato Compared to Synthetic and Natural Colorants", Food Chemistry, Vol. 86, No. 1, pp. 69-77 (2004).

[46] G. Calogero, J. H. Yum, A. Sinopoli, G. D. Marco, M. Grätzel, and M. K. Nazeeruddin, "Anthocyanins and betalains as light-harvesting pigments for dye-sensitized solar cells", Solar Energy, Vol. 86, no. 5, pp. 1563–1575 (2012).

[47] I. Konczak, and W. Zhang, "Anthocyanins: more than nature's colours", Journal of Biomedicine and Biotechnology, Vol. 2004, No. 5, pp. 241–242 (2004).

[48] N. Cherepy, G. Smestad, M. Graetzel, and G. Zhang, "Ultrafast electron injection: implications for a photoelectrochemical cell utilizing an anthocyanin dye-sensitized TiO_2 nanocrystalline electrode", The Journal of Physical Chemistry B, Vol. 101, No. 45, pp. 9342–9351 (1997).

[49] G. Calogero, and G. D. Marco, "Red Sicilian orange and purple eggplant fruits as natural sensitizers for dye-sensitized solar cells", Solar Energy Materials and Solar Cells, Vol. 92, No. 11, pp. 1341–1346, (2008).

[50] S. Hao, J. Wu, L. Fan, Y. Huang, J. Lin and Y. Wei, "The influence of acid treatment of TiO_2 porous film electrode on photoelectric performance of dye-sensitized solar cell", Solar energy Vol. 76, No. 6, pp. 745-750 (2004).

[51] H. Jeong, Y. Lee, Y. Kim and M. Kang, "Enhanced photoelectric efficiency by surface modification of TiO_2 thin film using various acidic species", Korean Journal of Chemical Engineering, Vol. 27, No. 5, pp. 1462-1468 (2010).

[52] W. Xu, S. Dai, and L. Hu, "Influence of different surface modifications on the photovoltaic performance and dark current of dye-sensitized solar cells", Plasma Science and Technology, Vol. 9, No. 5, pp. 556–559, (2007).

[53] F. Cao, G. Oskam, G. J. Meyer, and P. C. Searson, "Electron transport in porous nanocrystalline TiO_2 photoelectrochemical cells", Journal of physical chemistry, Vol. 100, No. 42, pp. 17021-17027 (1996).

[54] B. Kim, S. W. Park, J. Y. Kim, K. Yoo, J. A. Lee, M. W. Lee, D. K. Lee, J. Y. Kim, B. Kim, H. Kim, S. Han, H. J. Son, and M. J. Ko, "Rapid Dye Adsorption via Surface Modification of TiO_2 Photoanodes for Dye-Sensitized Solar Cells", American Chemical Society Applied Materials and Interfaces, Vol. 5, No. 11, pp 5201−5207, (2013).

[55] Q. Wang, J. Moser, and M. Gratzel, "Electrochemical Impedance Spectroscopic Analysis of Dye-Sensitized Solar Cells", The Journal of Physical Chemistry B, Vol. 109, No. 31, pp. 14945–14953 (2005).

[56] C.H. Hsu, and F. Mansfeld , "Technical Note: Concerning the Conversion of the Constant Phase Element Parameter YO into a Capacitance", Corrosion, Vol. 57, No. 9, pp. 747-748 (2001).

[57] C.C. Yang, H. Q. Zhang, and Y. R. Zheng, "DSSC with a novel Pt counter electrodes using pulsed electroplating techniques", Current Applied Physics, Vol. 11, No. 1, pp.

S147–S153 (2011).

[58] F. Fabregat-Santiago, J. Bisquert, E. Palomares, L. Otero, D. Kuang, S. M. Zakeeruddin, and M. Gratzel, "Correlation between Photovoltaic Performance and Impedance Spectroscopy of Dye-Sensitized Solar Cells Based on Ionic Liquids",
The Journal of Physical Chemistry C, Vol. 111, No. 17, pp. 6550-6560 (2007).

[59] R. Kern, R. Sastrawan, J. Ferber, and R. Stangl, "Modeling and interpretation of electrical impedance spectra of dye solar cells operated under open-circuit conditions", Electrochimica Acta, Vol. 47, No. 26, pp. 4213-4225 (2002).

[60] M. Zhong, J. Shi, W. Zhang, H. Han, and C. Li, "Charge recombination reduction in dye-sensitized solar cells by depositing ultrapure TiO_2 nanoparticles on “inert” $BaTiO_3$ films", Materials Science and Engineering: B, Vol. 176, No. 14, pp. 1115–1122 (2011).